This is a non-peer-reviewed preprint submitted to EarthArXiv.

What lies beneath: National aboveground carbon stock changes and under-canopy disturbance detection from 3D point clouds

Huntley Brownell[1*], Stefan Oehmcke[2,3], Thomas Nord-Larsen[1], Christian Igel[2]

[1*]Department of Geosciences and Natural Resource Management, University of Copenhagen, Rolighedsvej, Frederiksberg, 1958, Denmark.
[2]Department of Computer Science, University of Copenhagen, Universitetsparken 1, Copenhagen, 2100, Denmark.
[3]Institute of Visual and Analytic Computing, University of Rostock, Albert-Einstein-Straße 26, Rostock, 18059, Germany.

*Corresponding author(s). E-mail(s): hb@ign.ku.dk;
Contributing authors: stefan.oehmcke@uni-rostock.de; tnl@ign.ku.dk; igel@di.ku.dk;

Abstract

Accurate and spatially explicit quantification of forest biomass and carbon stock changes over time is necessary for carbon accounting and verification at different scales. Here, we applied deep learning to full 3D point-cloud data to produce a high-resolution time series of forest attribute maps for Denmark. The maps include predictions for biomass and canopy height with estimated uncertainties, spanning a decade from 2014 to 2024. By comparing to forest inventory estimates, we demonstrate that the maps can be used for national estimates of aboveground tree carbon stocks and stock changes. We benchmarked our maps against existing global and regional maps at varying scales and find that our maps are able to capture landscape-scale variation in both managed and unmanaged forests while retaining plot-level accuracy. Existing global and regional biomass mapping products often reduce forest structure to canopy-height metrics when estimating biomass, yet reliability of these proxies over time is largely untested. Given that most forests globally are managed, our analysis suggests biomass loss over time with steady or increasing canopy height is widespread, demonstrating that height change alone cannot reliably represent changes in forest carbon stocks.

Keywords: Aboveground biomass, Airborne LiDAR, Deep learning, Forest carbon monitoring, Canopy height, National forest inventory

Main

Forests are the largest terrestrial carbon sink, with most forest carbon stored in the combined pool of living biomass and the deadwood and litter produced by it [1, 2]. Globally, the forest sink has been stable over recent decades, but it is not uniformly distributed and may be at risk from deforestation and intensified disturbances; while the net sink is significant, it is only a fraction of the gross forest carbon uptake, so relatively small changes in fluxes could weaken it substantially [2, 3]. The size of the net sink is also uncertain. Widely cited studies estimate 1.33 ± 0.69 Pg C yr^{-1} between 1990 and 2019 [2] and 2.07 ± 13.4 Pg C yr^{-1} between 2001 and 2019 [3], the latter with an uncertainty more than six times the estimate. Reliable and spatially explicit knowledge of where carbon is stored in live biomass and how it changes over time is therefore central to monitoring Land Use, Land-Use Change and Forestry (LULUCF) contributions to commitments such as the Paris Agreement [4], and has long been a goal of scientific research.

Under the United Nations Framework Convention on Climate Change (UNFCCC), countries report LULUCF emissions and removals according to Intergovernmental Panel on Climate Change (IPCC) methods. These are

ORCID iDs: H. Brownell https://orcid.org/0000-0002-3798-8783 · S. Oehmcke https://orcid.org/0000-0002-0240-1559 · T. Nord-Larsen https://orcid.org/0000-0002-5341-6435 · C. Igel https://orcid.org/0000-0003-2868-0856

ranked in three tiers of increasing accuracy and data requirements: Tier 1 uses default values given by the IPCC by climate zone and forest type (for example, biomass stock and annual growth per hectare), Tier 2 replaces these with country-specific factors, and Tier 3 incorporates national measurement systems, such as national forest inventories (NFIs), or models [5]. The European Union's LULUCF Regulation, amended in 2023, sets a legally binding Union-wide target of 310 Mt CO_2-eq in net removals by 2030 and raises the reporting requirements, requiring geographically explicit land-use data and Tier 3 methods no later than 2030 [6, 7]. Increasingly, countries use NFIs for repeated sample-based measurement of forest attributes including biomass, although coverage, sampling density, and measurement quality remain uneven globally [8]. While NFIs are designed to provide statistically valid national estimates, the sample plots alone are too sparse to be used for mapping, though the data can be combined with remote sensing to produce national level maps. The IPCC has specifically noted that multi-temporal biomass maps could be used to estimate biomass change directly, but that the required accuracy to do so has not yet been achieved and that global maps often exhibit large and systematic errors [5]. Beyond national accounting, voluntary carbon markets have a pressing need for project accountability with demonstrably credible measurement [9–11]. This pushes the resolution and uncertainty quantification requirements for biomass mapping beyond the regional or country level to the forest level and below [12].

Despite ongoing efforts, existing biomass products from remote sensing still disagree substantially. Inter-comparisons of pan-tropical and global maps reveal pixel-level uncertainties on the order of 30–150 Mg ha^{-1} (comparable to typical forest-level biomass) along with strong and spatially-structured regional biases driven by sampling design, allometric assumptions, and the remote-sensing signals used as proxies [13, 14]. Global mapping products relying on space-borne sensors, such as the European Space Agency Climate Change Initiative (ESA-CCI) Biomass maps and the Gridded Aboveground Biomass Density maps from the Global Ecosystem Dynamics Investigation (GEDI), now provide near-global estimates with per-pixel uncertainty [15–18]. However, their native resolutions of 100 m to 1 km limit the potential to detect within-forest variability, knowledge of which is essential for actual forest management or verification. Recent introduction of higher-latitude LiDAR from the ICESat-2 programme shows promise for improving biomass mapping in areas without GEDI coverage [19], but closing the gap between coarse global accounting and operational sub-hectare estimation remains an open methodological challenge.

Airborne laser scanning (ALS) remains the only technology that can resolve three-dimensional forest structure in high detail across entire national territories [20]. The area-based approach is well established in the Nordic countries, in which summary statistics of the point cloud are regressed against NFI plots to produce wall-to-wall maps at 12.5–25 m resolution [21–23]. In Denmark specifically, successive national ALS campaigns (2006–2007 and 2014–2015) have been combined with NFI reference data to model wood volume and biomass, suggesting potential applications for both inventory reporting and forest management [24, 25]. Recently, ALS data have been used in combination with field data to calibrate space-borne LiDAR waveforms for estimating biomass [18]. However, in all cases, the full 3D structure of the ALS point cloud was condensed into a set of summary metrics, leaving much of the rich structural information contained in the original data unexploited.

Here, our research is motivated by the need to track forest structural change over time at high resolution for carbon stock monitoring and the production of forest maps that are accurate enough to be used by policymakers or forest managers. We show that a deep learning modelling framework utilising the full structure of the LiDAR point cloud provides a significant advantage over state-of-the-art methods that are limited by the reduction of complex forest structures to summary metrics, often reliant on canopy height. We demonstrate how canopy height is decoupled from biomass over space and time, making it unreliable for temporal carbon stock monitoring and under-canopy change detection. The maps and model we have produced offer potential for the improvement of regional and global mapping products by providing high-quality, continuous surfaces for benchmarking or training models that have not previously been available.

Time series of national maps

We obtained airborne LiDAR data from Danish national scanning campaigns covering the decade from 2014 to 2024. This represents two aggregated country-wide scans (hereafter national composites) and a partial third. Field plot measurement data from the Danish NFI [26] (n = 19,708 measurements at 13,350 plots) provided labels for training and evaluating a deep learning model employing 3D convolution with sub-metre voxels directly on the non-normalised point clouds [27]. We extended the existing method with quantile regression to provide prediction intervals [28–30], and retrained the model with additional data, learning a mapping from the raw point cloud to values for biomass, volume, canopy height, and basal area at a resolution equivalent to the NFI plot size (r = 15 m). We then applied the trained model to process the national point clouds after clipping to a tree-cover

mask (Methods) and sectioning the landscape into 15 m circumradius hexagons, the closest corresponding shape to the NFI reference data that can be tiled together.

The national maps (Fig. 1) consist of more than 22 million predictions over tree-covered areas in each of the composites. We also overlay national land-cover maps [32], to allow for analysis of tree biomass over different land-cover types. For comparison, the only global biomass time series with a resolution finer than 1 km is the ESA-CCI product [15, 33]. Coarser global products exist but would have limited utility for our purposes; proprietary maps have been developed but these are not publicly accessible or verifiable [12]. A series of European biomass maps at 20 m have recently been published for 2017, 2020, 2021 and 2023 [34], and we identified additional maps with a single reference year [19, 35–37]. For canopy height, single-year global and regional products are available along with a national sub-metre model [35, 38–42] (see Extended Data Table 1). We compared our biomass maps with the benchmarks by summing the predictions under two masks: the tree-cover mask, and a forest mask using relevant classes of the national land-cover maps, deriving national aboveground biomass (AGB) estimates both for forest areas and inclusive of trees outside forests (Fig. 2).

The true national total of tree aboveground biomass is unknown. Our estimates represent a masked wall-to-wall sum, while the NFI total is a sample-plot based statistical expansion. As NFI plots occur outside the forest areas of the land-cover map, the sampled area is not fully comparable to the forest mask; similarly, the tree-cover mask includes trees in areas which would not be sampled by the NFI, such as hedgerows or gardens. The model therefore offers potential for a more unified accounting of carbon stored in woody biomass across land-use classes, with the advantage of a single method applied to different land-use types (see Extended Data Fig. 1). This is especially relevant in countries where a significant portion of tree biomass exists outside of forest areas [35].

The time series of maps enables carbon stock change monitoring at any scale. Nationally, between the maps' mean acquisition dates (an approximately 6.6 yr interval) our model implies a net aboveground carbon stock change of $+2.9 \pm 1.2$ Tg C over the forest mask, inclusive of forest area change (Table 1). The annual stock change (each hexagon's change annualised over its own interval between scans) amounts to 1.66 ± 0.72 Mt CO_2 yr^{-1} over the forest mask and 2.35 ± 1.29 over the tree-cover mask; the NFI's 2.39 lies within the model's tree-cover mask interval and just above the model's upper bound over the forest mask (Table 1). The difference between our two masks, 0.69 Mt CO_2 yr^{-1}, is carbon accumulating in biomass outside areas classified as forest in the land-cover maps. For the ESA-CCI product, the annual stock change between 2015 and 2021 is 0.54 and 0.80 Mt CO_2 yr^{-1} under the same two masks (Table 1), 66–77% lower than our model and NFI estimates, though reported stocks are only around 30% lower. However, the ESA-CCI documentation advises caution when using the maps to assess AGB change [44] and notes that annual estimates are harmonised specifically to minimise inter-annual variability [45].

Table 1: **Aboveground tree carbon stocks, net stock change, and annual stock change.** All quantities refer to carbon in aboveground live-tree biomass. Stocks are reported over three populations: the land-cover forest mask, the tree-cover mask, and the NFI's own forest definition; the difference between the first two is biomass in trees outside forest. NFI estimates are from the Danish NFI's national statistics [43], interpolated to the composites' mean acquisition dates. Area is the extent of each population. Δ Stock is the simple difference between the two stocks, inclusive of area change. For our model, annual stock change annualises each hexagon's change over its own 5–9 yr scan interval, so it is not Δ Stock divided by the interval. The 95% CI for our model is internal systematic uncertainty estimated on held-out NFI plots. See Methods for details.

Source	Population	Area (kha)	Period	AGB-C (Tg C)	Δ Stock (Tg C)	Annual change (Mt CO_2 yr^{-1})
Our model	Forest (land cover)	651.9 → 664.4	2014–15 → 2019–23	29.5 ± 0.9 → 32.4 ± 0.9	2.9 ± 1.2	1.66 ± 0.72
ESA-CCI	(2015 → 2021)		2015 → 2021	21.2 → 22.1	0.9	0.54
Our model	Tree-cover mask	1299.2	2014–15 → 2019–23	38.0 ± 1.8 → 42.1 ± 1.6	4.1 ± 2.2	2.35 ± 1.29
ESA-CCI	(2020)		2015 → 2021	25.9 → 27.2	1.3	0.80
NFI	Forest (NFI definition)	624.8 → 651.7	2014–15 → 2019–23	33.1 → 37.4	4.3	2.39

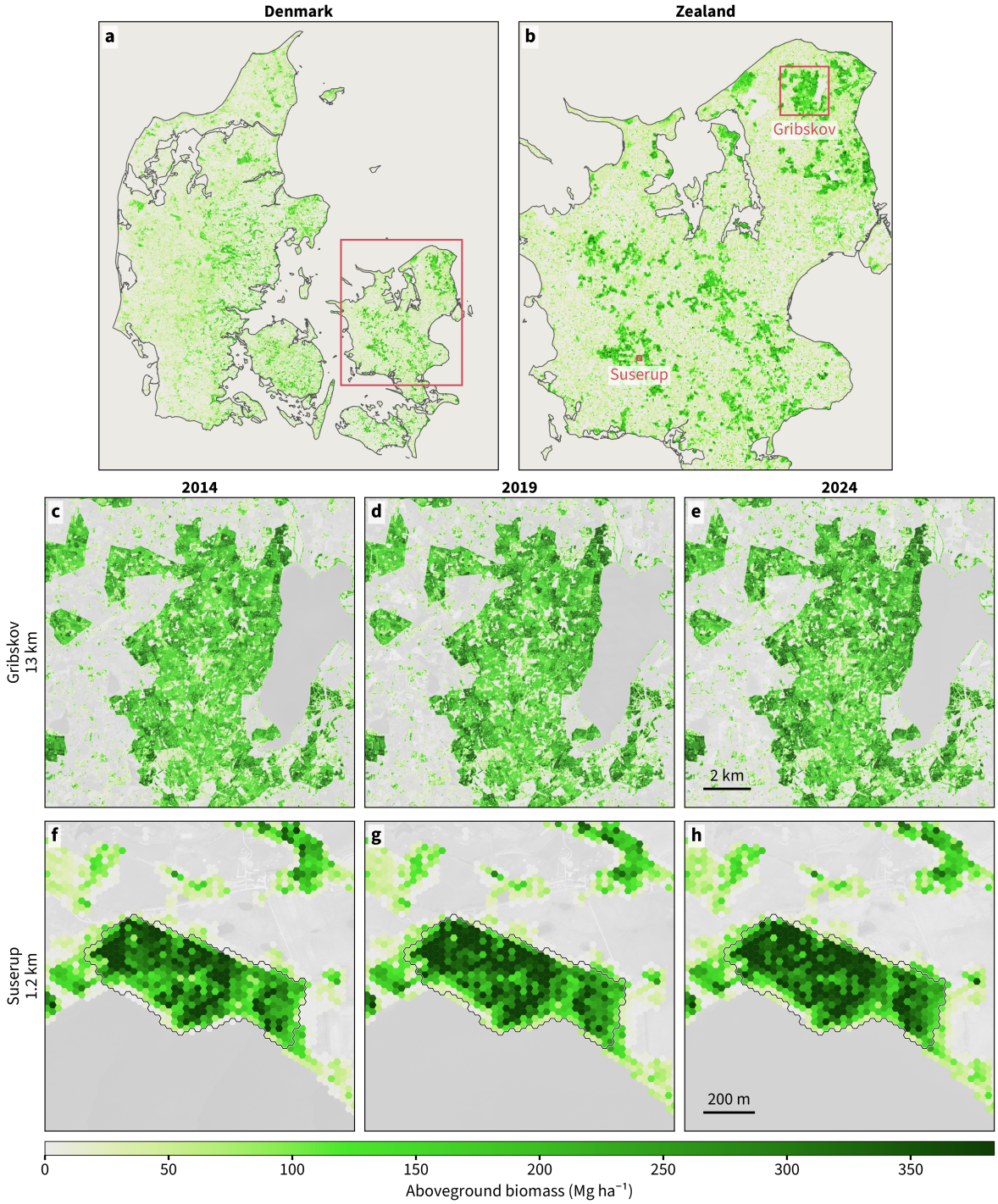


Fig. 1: **Tree aboveground biomass in Denmark.** (**a**) 5-year national composite from 2019–2023; (**b**) Zealand, showing location of forest insets of Gribskov and Suserup reserve. (**c, d, e**) Gribskov in 2014, 2019, and 2024. (**f, g, h**) Suserup reserve in 2014, 2019, 2024. Orthophoto basemaps contain data from Klimadatastyrelsen, GeoDanmark spring orthophotos [31].

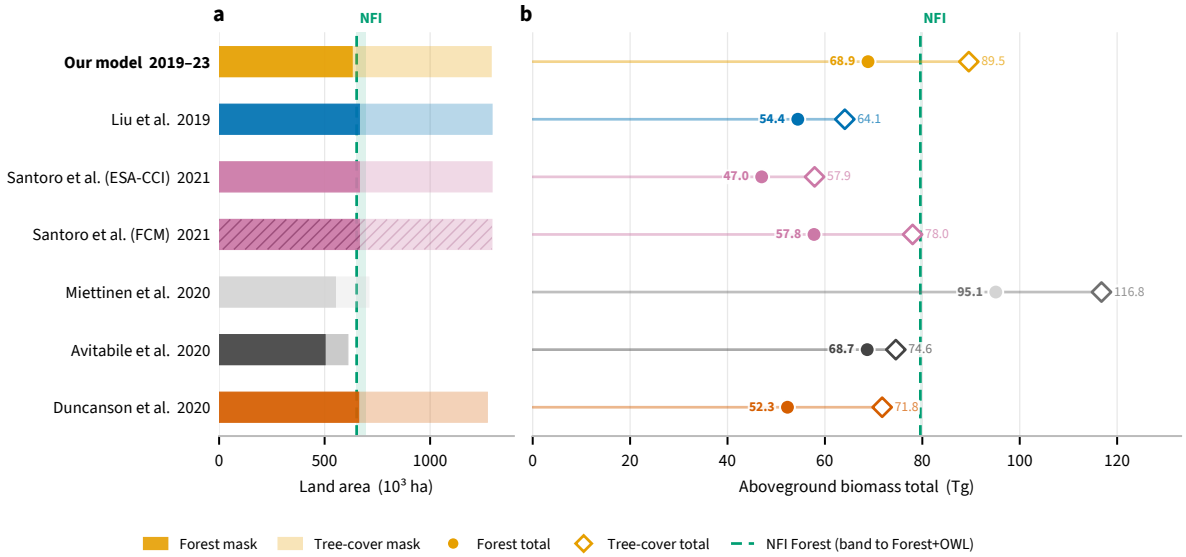


Fig. 2: **Danish national biomass totals.** Column **a** compares the land area in hectares over which each product has predictions under the forest mask (dark fill) and under the tree-cover mask (light fill). **b** shows corresponding national aboveground biomass totals with the filled circle showing the forest-mask total and the diamond the tree-cover-mask total. In both columns, the dashed green line represents the NFI estimate [43] for forest area, with the band extending to its forest + Other Wooded Land definition. Row labels give the year of each data product rather than its publication year; the benchmarks are Liu et al. [35], Santoro et al. (ESA-CCI) [33], Santoro et al. (FCM) [34], Miettinen et al. [37], Avitabile et al. [36] and Duncanson et al. [19]. Our model and the NFI estimate biomass over a 5 year cycle, so the equivalent midpoint year (2021) was used for both Santoro et al. benchmarks.

Local accuracy

While the overall national biomass totals derived from the benchmarked mapping products may reasonably agree with NFI estimates (or be calibrated to match them), this does not necessarily translate to local accuracy. Fine-grained biomass change detection would allow for transparent monitoring of tree carbon stocks for forest management and in projects affecting tree cover, such as for afforestation, rewilding, or restoration purposes, an outstanding need [46].

To evaluate local accuracy of the maps, we investigated model performance across forest areas under different management regimes. We used as references both an unmanaged forest reserve and a forest estate managed with multiple goals, including timber production and biodiversity conservation. For ground truth, we obtained a time series of individual tree measurements (most recent census $n = 10{,}851$) in the Suserup forest reserve (≈ 24 ha) and high density sample-plot ($n = 268$) based forest inventory, covering 148 ha, for the managed Frederiksdal forest estate (≈ 200 ha of forest). We compare our model to the field measurements and other available benchmarks; by taking the mean value across pixels, we are able to compare products of different native pixel resolutions, ranging from 0.4 m to 100 m (Fig. 3).

In general the models perform better in the more homogeneous managed forest. In the unmanaged reserve, all models underestimate biomass relative to the ground truth, with the global and regional products underestimating by more than 50% in some cases, while our model is within 20% of recorded field values in the most recent census.

It is widely known that remote-sensing products can saturate at higher biomass values, but here some of the benchmarked models consistently estimate similar or lower overall biomass in the reserve than is found in the managed forest, even though the field-measured mean biomass in the reserve is 30–60% higher. Estimating the full vertical vegetation structure from two-dimensional imagery is challenging, and estimates that take only canopy cover and tree height into account are not sensitive to understory differences in biomass. The difficulty of using remote-sensing methods (including GEDI-derived canopy height) to detect carbon stock differences in managed/unmanaged forest pairs was also recently reported in Belgium [47]. This suggests that existing models may not resolve areas of atypically high biomass within a landscape, which should be investigated further, particularly if a long-term goal of such maps is to identify areas with high biomass for conservation of aboveground carbon stocks or for biodiversity protection. Recent work combining Sentinel-2 imagery with GEDI height profiles to map the full vertical vegetation structure globally found that the combination identifies natural forests better than canopy height alone [48], pointing to the need for richer structural information in biomass mapping.

While forest-level mean attributes describe the forest more broadly, higher-resolution data is necessary to capture within-forest variation, particularly important for change or anomaly detection that may contrast with general trends. In our managed forest reference, we find that the maps are able to resolve forest change in line with inventory plots and management records, indicating that biomass growth and removal are consistently observed (Fig. 4; Extended Data Fig. 2). Here we also observe that correlated forest attributes, such as biomass and canopy height, can move in different directions.

Canopy height is an unreliable biomass proxy over time

An often-used proxy to derive biomass is canopy height, with the underlying assumption that across space and time increasing canopy height represents monotonically increasing biomass, all things being equal. This is well founded in principle and the trend can be demonstrated cross-sectionally in any static dataset of canopy height and biomass. However, we suggest that high-resolution time-series data causes this assumption to collapse, because "all things being equal" cannot hold over time and space, particularly in cases where human management of forests occurs. Management often translates to removal of trees (i.e., a reduction in density) while leaving the canopy intact, and as biomass is a function of both height and density, the relationship between canopy height and biomass is not consistent under management.

According to one estimate [49], a minority ($\approx 40\%$) of the world's forests are unmanaged natural forests; in Europe most forests are subject to management, with only a very small percentage ($\approx 2\%$) protected from human intervention [50]. This implies that over time, at a given location, most forests will not have a consistent relationship between biomass and canopy height. This could become increasingly true in the future if forest management continues to shift away from even-aged rotation forestry with a clearcut system to uneven-aged forest management under a continuous tree canopy. While canopy loss has been used for global forest change detection [51], it has also been widely recognised that tropical forest areas are subject to selective logging and other smaller scale disturbances [52–54] which may not be reflected in canopy height.

Our time series of 3D data makes it possible to demonstrate that at a fixed location over time, canopy height is often decoupled from biomass. That is, at the local level the canopy height can increase or remain steady while the

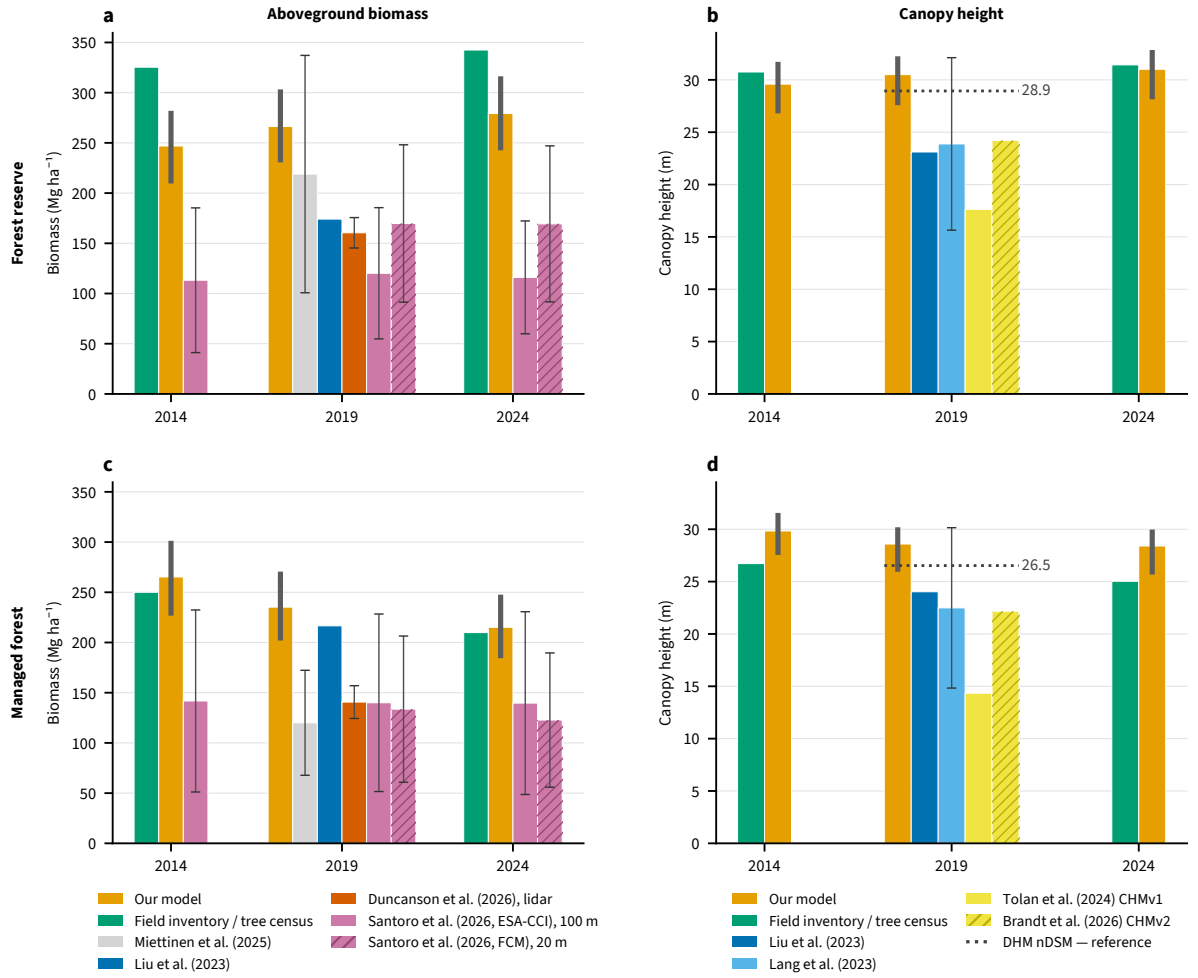


Fig. 3: **Local validation: model vs field and benchmarks in unmanaged and managed forests.** Model mean biomass and canopy-height predictions benchmarked at the forest level against an all-tree census in unmanaged forest reserve (**a**, **b**) and sample plot inventory in managed forest (**c**, **d**). In both locations LiDAR data were available for 2014, 2019, and 2024. Field measurement campaigns occurring within a year of the LiDAR scans are shown, with other remote-sensing products (co-occurring within one year) also included according to availability along with reported uncertainty: for our model the mean predicted interquartile range (Q25–Q75) of the hexagon predictions, and for benchmarks that publish per-pixel uncertainty, ± the site-mean pixel standard deviation. In (**a**) we see that in the unmanaged forest reserve all remote-sensing products underestimate biomass according to ground truth, though our model comes the closest to the field census. (**b**) includes the 0.4 m resolution normalised digital surface model (nDSM) from the Danish elevation model (DHM) which uses the terrain model and surface model to derive canopy height. Here the model is closest to both the DHM and field measurement reference. In (**c**, **d**) the model and Liu et al. are most closely aligned with the sample-plot based field inventory.

biomass decreases. In Fig. 4 we highlight an example of this occurring in a single forest stand of 12 ha in our managed forest reference, where canopy height increases monotonically from 2014 to 2024, while biomass increases and then falls: between 2019 and 2024 modelled aboveground biomass fell from 304 to 257 Mg ha^{-1} while canopy height continued increasing from 29.6 to 30.3 m. These numbers are consistent with known management activities as a selective removal of trees (a thinning) was carried out here in the winter of 2022–23.

We see the pattern in other stands (for an estate-wide biomass map, see Extended Data Fig. 2); between 2019 and 2024, 138.7 ha (76%) of the forest lost modelled biomass, and in just under half of that area (∼64 ha) the loss occurred while canopy height held steady or increased (mean increase of ∼0.4 m). This amounts to a biomass loss of ∼1,700 Mg AGB which a canopy-height proxy would not register.

We confirm this pattern at national scale using the subset of remeasured permanent plots from the Danish NFI: across 9,469 plot measurements in 2,650 plots, the height–biomass relationship is strong ($r = 0.77$), but it weakens substantially within plots over time ($r = 0.51$, $n = 7{,}250$ paired remeasurements). For plots where

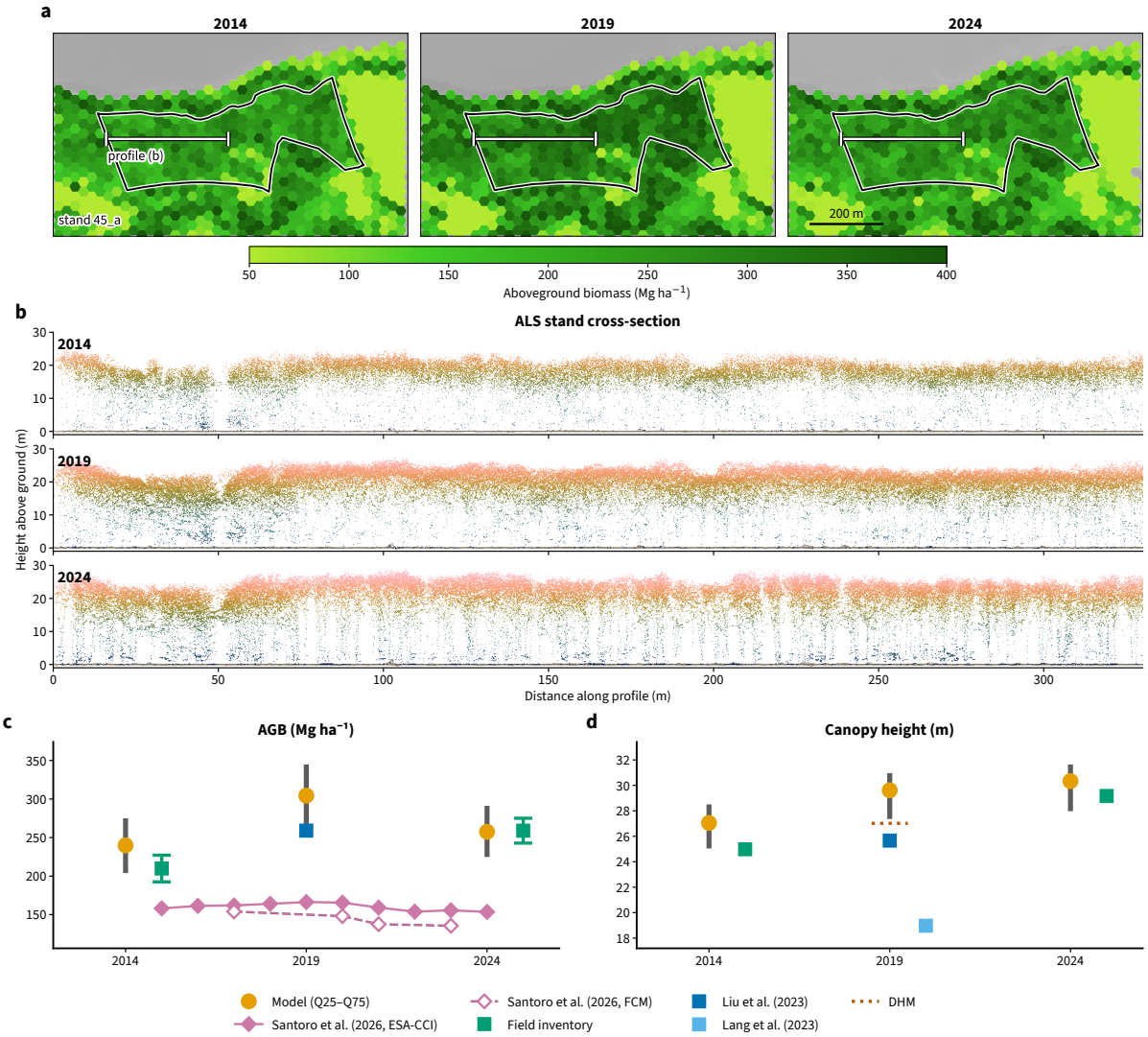


Fig. 4: **Model shows biomass decreases while canopy height increases following management in our managed forest reference. a**, Modelled biomass from 2014–2024 in the example compartment (outlined) in the managed reference forest (Frederiksdal, see Extended Data Fig. 2). **b**, LiDAR cross-sections along the profile marked in **a**. **c**, Model and benchmarks for aboveground biomass: modelled biomass decreases between 2019–2024, after recorded tree removal (thinning targeting 20–30% of standing volume) in 2022–2023. Field inventory in 2015 and 2025 brackets the decline but has no 2019 measurement. **d**, Canopy height increases in field inventory and model. Error bars: model, stand means of the hexagons' predicted 25th and 75th percentiles (Q25–Q75); field inventory, ±1 standard error of the mean of the stand's six inventory plots.

field-measured biomass declined by more than 2 Mg ha^{-1} between surveys, in 57.8% of them canopy height held steady or increased ($\Delta h_{\text{can}} \geq -0.5$ m), suggesting that more than half of the plots with measured biomass losses nationally would have been missed by a height-only change signal. These plots account for 38% of the field-measured biomass loss, as larger losses more often lower the canopy. If we further examine our national modelled biomass predictions between composites, we find a similar fraction: over the forest mask, 64.6% of hexagons with a modelled biomass decline of more than 2 Mg ha^{-1} also show steady-or-rising modelled height, on the same criteria. In 94% of these hexagons modelled basal area also declined, consistent with tree removal beneath an intact canopy.

Time series of earth observation products are now generally available, and have been used to monitor land-cover change and forest loss by detecting changes in the tree canopy [51, 55, 56]. However, high-resolution time-series maps of canopy height and other forest attributes are rare; a recent study suggests optical products need to be of very high resolution (1.5 m) to enable accurate detection of disturbances affecting canopy height in intact forests [57]. The remote-sensing literature has long recognised that the relationship between biomass and height is sensitive to various structural factors, but the focus has often been on model transferability across different biomes

or regions of sensor coverage and overall prediction accuracy. This focus on overall static accuracy may neglect confounding relationships across space and time, particularly relevant in environmental monitoring [58]. It has also been recognised in ecology that the substitution of a spatial gradient for a temporal one can be misleading or result in spurious conclusions [59–61].

Time series are further complicated when the potential rate of change is asymmetrical [62]. Increases in biomass and canopy height are limited by the speed of the underlying natural growth processes. However, reduction of biomass and canopy height can occur very rapidly, while recovery from these events remains rate-limited. The assumption of covariant monotonic increase in biomass and height potentially misses rapid change in the other direction, which is critical for change detection. For carbon projects, which can be certified in managed as well as natural forests [63], it is important to be able to accurately account for localised changes in carbon stocks, especially as cumulative CO_2 removal over time for a given forest area can increase with repeated removal and regrowth of biomass when harvested wood product storage is accounted for [64].

Comparison of landscape-level variation

While coarser-resolution products may have limited use for localised change detection, we were also interested in the ability of the models to capture structural texture across larger forest areas, since both vertical and horizontal variation is associated with forests of higher biomass and biodiversity [65, 66]. We therefore aggregated model predictions to a grid corresponding to the lowest resolution product (100×100 m) for analysis. The differences between the models are visually apparent (Fig. 5), and even more so at each product's native resolution (Extended Data Fig. 3).

Since a noisy model could produce the appearance of variation, we further compared the products by sampling each map at NFI plot locations not used in the training of our model (see Table 2). For evaluation we used Pearson's correlation coefficient r and Spearman rank correlation ρ as they allow for comparing model performance without unfairly penalising them for bias due to a lack of local calibration. Pearson's is invariant to affine (bias and scale) differences so evaluates potential model skill after linear recalibration, while Spearman's is invariant to any non-linear order-preserving miscalibration (i.e., relevant in this case to potentially account for non-linear bias, such as saturation at high biomass values). R^2 incorporates these biases, which disadvantage the global and regional models. However, both r and ρ show the gap between our model and the other products is not only a calibration artefact, since it cannot be removed by rescaling.

If each product were locally recalibrated to remove affine biases the theoretical maximum of the best performing benchmark is $R^2_{\text{max}} = r^2 \approx (0.73)^2 \approx 0.53$ as compared to $R^2 = 0.845$ for our model without recalibration (see Table 2). While it was expected that a coarser biomass product would not be able to capture as much variation, several of the models do not capture the variation better than a mean prediction. Three of the biomass benchmarks (Santoro et al. (ESA-CCI), Avitabile et al. and Miettinen et al.) cluster at $r = 0.42$–0.43 with negative or near-zero R^2 and systematic biases of 10–61 Mg ha^{-1} against a field mean of 97.7 Mg ha^{-1} that dominate their error relative to predicting the field mean. Liu et al., the space-borne LiDAR product (Duncanson et al., ICESat-2) and the 20 m Santoro et al. (FCM) product are the exceptions, reaching positive R^2 while still carrying biases of -27, -21 and -22 Mg ha^{-1}.

The coarser products especially are affected by pixel-support mismatch with larger pixel sizes which could average over landscape-level variation (see Extended Data Fig. 4). Taken together, the landscape map comparison (Fig. 5) and test-plot comparison (Tab. 2 and Fig. 6) illustrate the importance of capturing landscape variation for overall accuracy. When it comes to canopy height, performance is much improved, however the relatively large biases still affect performance. Plotted against field measurements, the models appear internally consistent in trend but the biases are readily apparent across biomass ranges (Fig. 6).

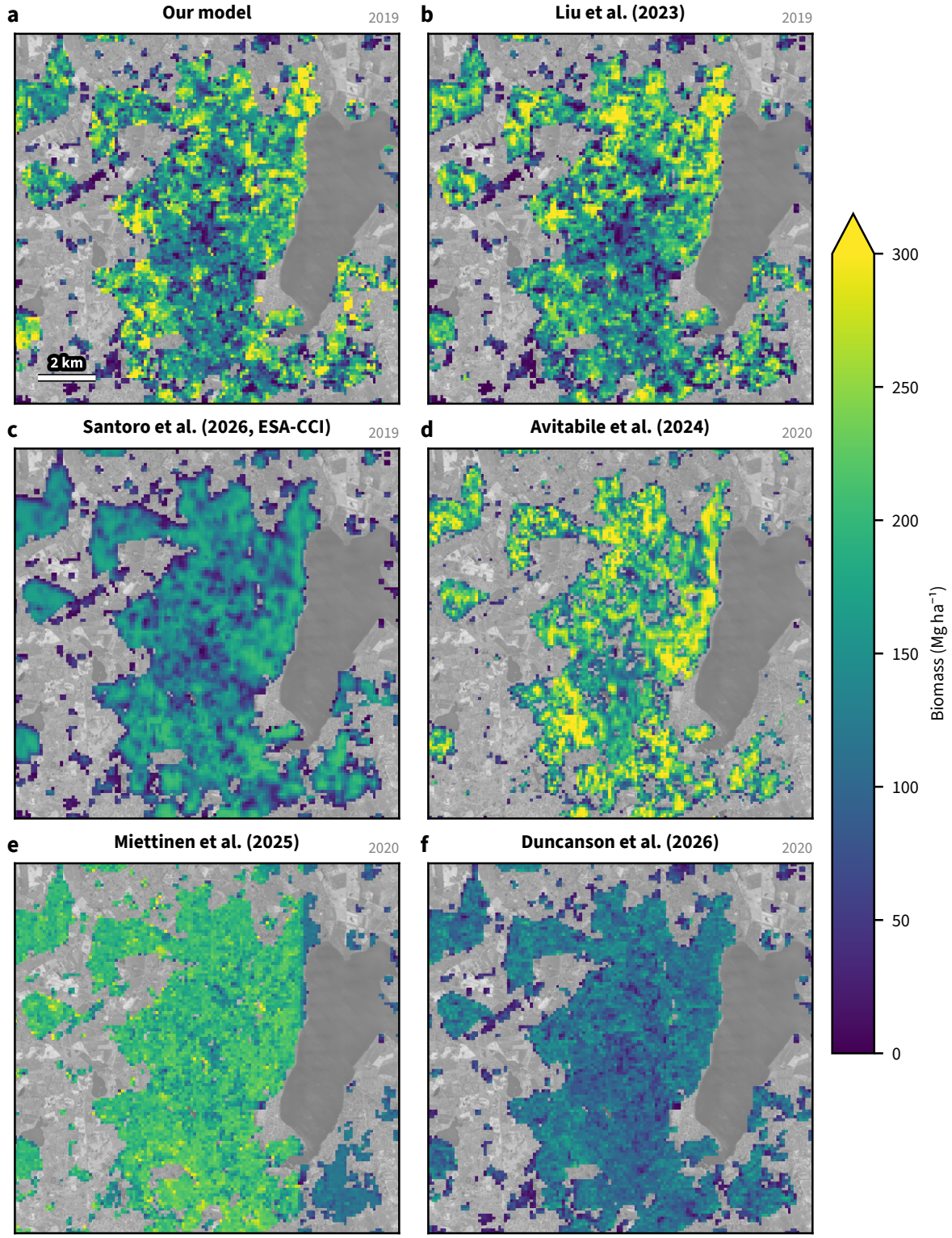


Fig. 5: **Same forest but different maps: model textural variation at landscape scale (approx.** 13×13 **km). a** (our model) and **b** (Liu et al. [35]) appear to exhibit similar biomass range and spatial variation, while **c** (Santoro et al. [33]) exhibits saturation or scaling that limits higher biomass values. **d** (Avitabile et al. [36]) is based on **c** rescaled and resampled based on national totals, and seems to overestimate across the landscape. **e** (Miettinen et al. [37]) suggests compression towards moderate levels of biomass with lower and higher values largely absent, with a shift in range where Sentinel-2 tiles join visible towards the right side of the panel. **f** (Duncanson et al. [19]) exhibits variation yet does not detect high biomass areas. For native resolutions, see Extended Data Fig. 3. Orthophoto: Klimadatastyrelsen [31].

Table 2: **Plot-level benchmark against NFI field measurements** in the common 2019–2020 temporal window shared by all models ($n = 147$ held-out test plots). Coverage = fraction of the 147 plots for which the product provides a prediction (some are masked and some are fully wall-to-wall); a product with coverage $< 100\,\%$ has spatial gaps at the remaining plots. r = Pearson correlation; ρ = Spearman rank correlation (Pearson r of the ranks); R^2 = coefficient of determination; Bias = mean (signed) error. The three performance metrics are complementary; r is invariant to a global bias-and-scale (affine) recalibration, ρ additionally forgives any monotone nonlinearity such as saturation, and R^2 penalises absolute calibration error (bias) on top of ranking.

Product	n	Cov. (%)	r	ρ	R^2	RMSE	Bias
Aboveground biomass (Mg ha^{-1}; field mean 97.7)							
Our model	**143**	**97**	**0.920**	**0.904**	**0.845**	**35.4**	−3.7
Duncanson et al. (2026)	147	100	0.728	0.766	0.417	68.8	−20.6
Santoro et al. (2026, FCM)	147	100	0.641	0.649	0.346	72.9	−21.7
Liu et al. (2023)	147	100	0.621	0.702	0.295	75.7	−26.9
Miettinen et al. (2025)	130	88	0.430	0.482	−0.284	101.8	+60.7
Santoro et al. (2026, ESA-CCI)	147	100	0.426	0.483	0.002	90.0	−38.0
Avitabile et al. (2024)	120	82	0.420	0.408	−0.006	90.5	−10.1
Canopy height (m; field mean 17.0)							
Our model	**143**	**97**	**0.952**	**0.945**	**0.905**	**2.7**	+0.3
Brandt et al. (2026)	147	100	0.815	0.815	−0.185	9.9	−8.2
Liu et al. (2023)	147	100	0.766	0.766	−0.023	9.2	−7.0
Lang et al. (2023)	147	100	0.698	0.680	0.483	6.5	+0.6

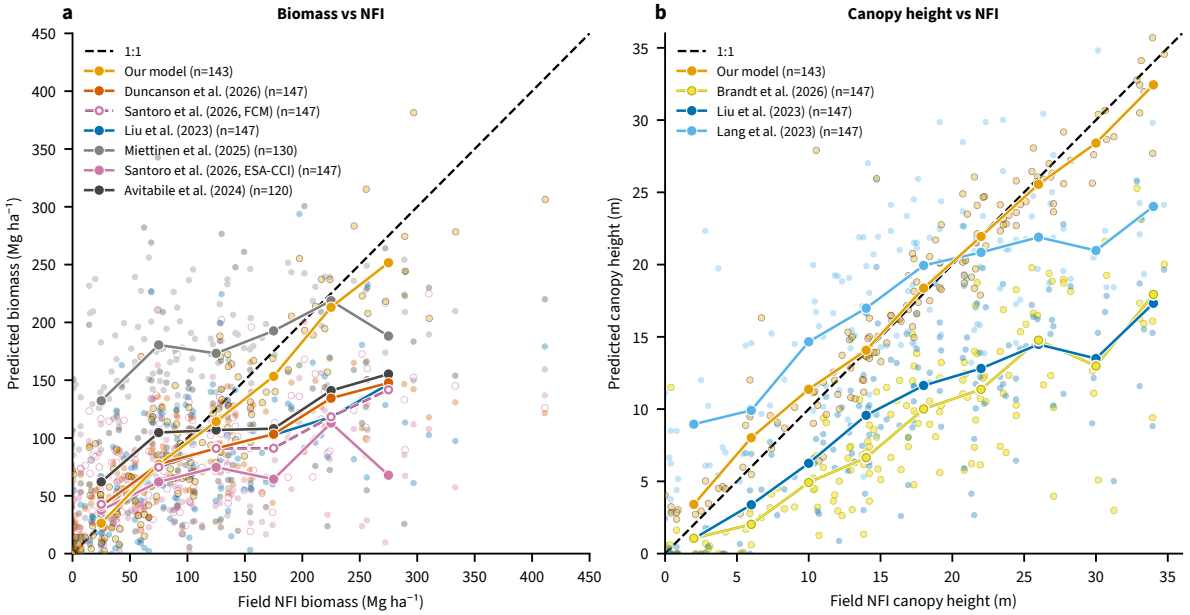


Fig. 6: **Plot-level agreement with NFI field measurements at held-out test plots.** Predicted against field-measured aboveground biomass (**a**) and canopy height (**b**) for our model and the benchmark products at the 147 test plots measured in 2019–2020 (Table 2; temporal matching in Methods). Points are individual plots; lines join the mean prediction in each bin of field value (50 Mg ha^{-1} in **a**, 4 m in **b**; bins with at least three plots).

Perspectives on biomass mapping and scalability

To the best of our knowledge, the maps presented here are the first time series of national maps of tree aboveground biomass, volume, canopy height, and basal area derived directly from full 3D point clouds. While the biomass and volume predictions are based on Danish allometric functions underlying the NFI, canopy height and basal area are not derived but are measured quantities in the ground truth, meaning that model performance could be evaluated wherever there are LiDAR scans with accompanying field measurements.

The resolutions of the maps we have benchmarked here vary; however, we have shown that at the landscape and forest level their practical utility for spatial evaluation of biomass stocks is limited, either because they do not capture variation or because they carry strong biases, even where their national totals are close to inventory estimates. We emphasise that our intent is not to criticise the existing regional and global products; the challenges involved in developing a global model are vastly greater than for a national one, and the developers of these models generally acknowledge their limitations. We prefer to highlight the potential for demonstrably accurate national maps to be used for improvement of other products.

One of the biggest obstacles that must be overcome when producing regional and global maps is the highly sparse nature of ground-truth data, particularly in the global south [15]. Even within a well-sampled region such as Europe, existing data for calibration are often difficult to access. LiDAR has contributed to filling these gaps; global maps are often calibrated using GEDI data, but the GEDI footprints are themselves sparse and restricted to between 51.6° N and 51.6° S (i.e., excluding Denmark and much of northern Europe). High-resolution national products of the type we present here can serve as spatially-dense data needed to retrain the retrieval algorithms behind global and regional products, addressing the reference-data sparsity problem.

Though products issued for a single reference year have proven to be useful benchmarks, efforts should be focused on reproducible methods that can be used to produce reliable time series, as land management for climate change mitigation demands accurate quantification of change over time. It is not surprising that using full 3D structural information should provide a better result; the next best performing model in our study (Duncanson et al., ICESat-2) incorporated relative height metrics from LiDAR in addition to canopy top height, suggesting the importance of deriving structure using active sensors.

LiDAR data is now available for a number of countries in Europe; we will publish our pre-trained model weights upon acceptance so that the model may be applied to other areas with fine-tuning or validation. This should enable significantly more accurate regional estimations. Others have proposed that LiDAR reference data is the only suitable ground-truth reference to calibrate remote-sensing products, as individual plot estimates can be biased and the number of plots required to reduce this bias to acceptable levels is not feasible [67]. A globally distributed network of reference areas including airborne LiDAR has been proposed [68] and a dataset of LiDAR-derived canopy height has recently been published [69]. This offers potential for reference data far beyond what was formerly available; further extending this data with a method such as ours that can utilise the full point-cloud structure below the canopy would offer greater potential for accurate assessment of forest and biomass change over time.

Methods

LiDAR and label data

We used national composite point clouds collected across multiple ALS acquisition campaigns [70]. The first scan was completed during 2014–2015 with approximately half of the country scanned each year, and during the second composite, 2019–2023, approximately $1/5$ of the country was scanned each year. The campaigns continue, and we utilised scanning data from 2024 to enable a third series for areas of interest. The point clouds were collected with different sensors and scanning patterns, with point densities increasing over time. In our training samples, the median number of returns per m^2 increased from 13.7 to 32.1 between the first and second composites. The points carry metadata such as intensity, return order, and classification, but only XYZ coordinates were used during training. The total size of the point cloud from 2014–2015 is 2.1 TB while the 2019–2023 cloud is 16 TB.

The label data originates from the Danish NFI, carried out by the University of Copenhagen during the years 2002–2023, from which we used plot-level attributes: biomass ($Mg\,ha^{-1}$), volume ($m^3\,ha^{-1}$), canopy height (m), and basal area ($m^2\,ha^{-1}$). The circular sampling plots have a radius of 15 m ($A \approx 0.0707\,ha$), consisting of three concentric circles of 3.5, 10, and 15 m radius, in which all trees, trees $>$10 cm diameter (at breast height of 1.3 m, or DBH), and trees $>$40 cm DBH are measured, respectively [26]. Per-plot biomass and volume were calculated based on diameter measurements and measured or estimated heights of individual trees, to which allometric equations were applied; basal area is calculated from measured tree diameters. Plot-level estimates are scaled to represent a per-hectare rate [26]. The inventory data was filtered to retain only plots where the innermost circle of the nested inventory design had $\geq$ 50% forest cover. We were interested in retaining plots falling at the forest edge, but as trees less than 10 cm DBH are only recorded in the centre circle and extrapolated to the outer circles for plot-level estimation, an unforested plot centre could omit any smaller trees from being tallied and bias the extrapolation of individual tree measurements to per-hectare totals.

From each national composite, point clouds corresponding to the locations of the filtered inventory were extracted. Since the inventory dataset contains more than 20 years of measurement data, this meant that some

locations had a 20 year gap between measurement and scan, and some measurements were taken up to 9 years after scanning. As the temporal gap increases the labels become noisier owing to both natural and anthropogenic processes; among these, tree growth occurs during each growing season, and the probability of management (i.e., removal of trees) occurring increases with time elapsed. To minimise label/cloud drift while retaining a sizeable dataset, we opted to use label/cloud pairs with a time difference of ≤ 5 years. Cloud/label pairs with a smaller temporal difference were considered less likely to suffer from a mismatch owing to growth or removal of trees, so were judged more reliable for validation during training and reporting model performance. We therefore sorted the available data by time difference between field measurement and scan: point-cloud/label plot pairs with a time difference < 1 year were divided between all splits (training, validation, calibration and test), while plots with a time difference ≥ 1 year were only used in the training set. Unique plot locations only appeared in one set.

Model architecture, training, and initial bias correction

We build on the sparse 3D convolutional MSENet50 architecture [27], implemented with MinkowskiEngine 0.5.4 [71], which operates directly on non-normalised point clouds. After clipping to 15 m circumradius hexagons in order to match the intended mapping application, the point clouds were randomly downsampled to $n_{\max} = 16{,}000$ (see Extended Data Fig. 5 for effect of downsampling on point-cloud structure) and then quantised to a sparse voxel grid (grid size 0.0125 in normalised model units, i.e. 0.375 m in x and y and 0.5 m in z, as the axes are normalised by 30, 30 and 40 m respectively) using only the XYZ coordinates, from which the three input features per voxel (scaled height z, a constant, and horizontal distance to the plot centre) were derived. Other available attributes (intensity, return number, classification) were not used during training, and points classified as human-made structures were filtered out before downsampling. The backbone produces a 2048-dimensional embedding by sum-pooling over the final sparse feature map.

To predict the four forest attributes (plot aboveground biomass, volume, canopy height, basal area) together with prediction intervals, a single linear regression head maps the 2048-d embedding to twelve standardised outputs – for each attribute a point estimate and the 0.25 and 0.75 conditional quantiles. The training objective is a composite of a Huber loss [72] on the four point outputs and pinball (quantile) losses at $\tau = 0.25$ and $\tau = 0.75$ on the corresponding quantile outputs [30]. The two quantile outputs give a nominal 50% (interquartile) prediction interval for each attribute.

Models were trained for 310 epochs on a single NVIDIA A100 GPU, with pre-processing, augmentation and other hyperparameters set as in Oehmcke et al. [27], followed by batch-normalisation recalibration of 20 epochs with fixed weights. We trained 6 independent runs (training time $\approx$ 36 hours) and selected the model with the highest validation ($R^2 = 0.83$) score on the biomass target.

Unlike with the ordinary least-squares method, when training deep learning models for regression it cannot be expected for residuals on training and validation data to sum to zero; this can introduce an additional bias, and when summing predictions over large areas it can accumulate [73]. We therefore used the training and validation plots measured within one year of their scan to apply a bias correction (calculated separately for each national composite; the partial 2024 campaign has no plots of its own and uses the 2019–23 correction) to all downstream predictions. We used the median rather than mean bias to minimise the effect of large outliers which could occur from cloud/label mismatches given the temporal gap between scan and measurement, for example, if trees were removed in this interval.

We used the held-out calibration set after removal of label mismatches (remaining $n = 761$) to evaluate nominal quantile coverage, finding that the model was globally well calibrated and close to the nominal 0.50 for every attribute (aboveground biomass 0.54, stem volume 0.52, canopy height 0.58, basal area 0.50) and stable across forest types. At the highest biomass densities (> 300 Mg ha^{-1}) the conditional coverage degraded (AGB 0.32, stem volume 0.27, basal area 0.29; canopy height unaffected at 0.66), indicating that the intervals become overconfident where the mass-related attributes saturate.

Finally, we evaluated the selected model on the fully held-out test split, from which no plots were used in training or model selection (Extended Data Table 2). The model captured most of the plot-to-plot variance in every attribute (test R^2 0.77–0.93, highest for canopy height), with relative RMSE ranging from 13% for canopy height to 31–35% for the mass-related attributes. Residual per-plot bias after the correction was small and, for aboveground biomass and stem volume, statistically indistinguishable from zero (Extended Data Table 2). The bias correction changes R^2 by less than 0.002, and excluding the 29 label/scan mismatches raises it by 0.02–0.06 (Extended Data Table 3). Performance on the validation split used for model selection was near-identical (biomass $R^2 = 0.83$; canopy height $R^2 = 0.93$), indicating that model selection did not overfit the validation data.

National maps: carbon stocks, stock changes, and uncertainty

The selected model was applied to the national point clouds using a tree-cover mask, with the country divided into sub-grids for processing. The tree-cover mask is derived from a 10 m random-forest classification of 2020 Sentinel-1 and Sentinel-2 imagery trained on NFI plots [74], converted to polygons, with a 20 m buffer applied; it therefore includes small tree-covered areas outside forest and a margin around all tree cover. The total runtime across the three acquisition campaigns was approximately 1,130 GPU-hours (2014–15: 272; 2019–23: 622; partial 2024: 237). Per-task runtime was dominated by loading the 1×1 km LiDAR tiles (.las format) rather than model inference. Computational cost scaled approximately linearly with point density: the 2019–23 point clouds required roughly $2.2\times$ more processing time per tile than the 2014–15 data, consistent with the approximately $2.3\times$ increase in median return density (from 13.7 to 32.1 returns m^{-2}). The resulting point predictions are tiled into hexagons with a 15 m circumradius, with more than 22 million predictions for each national composite.

These predictions are summed under two masks, the tree-cover mask (1,299,183 ha as tiled by the hexagon grid, with the same mask from 2020 used in both national composites) and a forest mask (the Forest and Christmas-tree classes of the land-cover maps; 651.9 kha in 2015 for the first national composite and 664.4 kha in 2021, for the second national composite). This gives stock totals across both composites for both masks. The forest mask comes from the Danish national land-use/land-cover maps used for UNFCCC LULUCF reporting [32]: 25 m rasters (ETRS89 / UTM zone 32N) of seven land-use categories based on the IPCC classes, derived from national topographic and agricultural registers and updated annually. We used the 2015 and 2021 layers to match the two composites, and assigned each hexagon the class of the pixel containing its centroid. Biomass was converted to carbon (C) with a factor of 0.47 and C to CO_2 with $44/12$.

We report two measures of change, using different calculation methods: the net stock change and the annual stock change. The net stock change between the two national composites ($+2.9 \pm 1.2$ Tg C in the case of the forest mask) is the simple difference between each composite's stock total, summed over all hexagons for each mask. It is therefore inclusive of forest-area change within the masks between the two composites (Table 1). However, to calculate the annual stock change, we restrict the calculation to hexagons with a valid prediction in both national composites and an assigned acquisition date. This excludes 0.7 % of the second composite's hexagons under the forest mask and 1.0 % under the tree-cover mask, mostly data gaps in either composite. We also consider each point's acquisition date, since the individual scan intervals range from 5–9 years depending on location. The overall population is split into cohorts by interval; the annual stock change is therefore the sum of each cohort's (g) own annualised change: $\sum_g \Delta\mathrm{AGB}_g / \Delta t_g$. The NFI national totals are the inventory's annual series of national estimates [43], each pooled over a five-year measurement cycle; the annual values between the report's five-year intervals were provided by the NFI. For Table 1 we assigned each to the midpoint of its cycle and interpolated linearly to the mean acquisition dates of our two composites (mid-2014 and early 2021, 6.6 yr apart), so the NFI's net and annual stock changes cover the same interval as our model.

Uncertainty for a national total summed over millions of predictions is dominated by systematic error rather than random error, which would cancel over $\approx 2 \times 10^7$ hexagons in each composite. Such a systematic bias scales with the area it is summed over, as discussed above in the application of deep learning for regression. For the purpose of estimating the national-level uncertainties for stocks and stock changes we therefore use the held-out calibration and test plots to estimate systematic error. We take the mean residual (prediction $-$ field) over bins of predicted biomass (0–50, 50–100, 100–150, 150–200, 200–300, $>$300 Mg ha^{-1}) weighted by the area of each bin in each mask, to reflect the biomass distribution of the national maps rather than that of the plot sample. As the two masks describe different populations (forest land cover and tree crowns nationally) we account for this in our estimation procedure.

For the forest mask we use the held-out NFI plots that fall within the mask; for the tree-cover mask we use the plots from within the forest areas but also the $\approx$ 14% of NFI plots falling outside of the forest mask, each weighted by their representative area within the tree-cover mask. The standard error (for the two stock changes, the standard error of the composite-to-composite difference) comes from a cluster bootstrap resampling NFI plot clusters across composites. Since 10% of held-out plots appear in both composites, the joint resampling captures covariance rather than treating each map as fully independent. These intervals describe our model's error relative to the NFI plots only. They do not include error in the allometric models and methods behind the NFI, which our model shares through its training labels, nor, for the tree-cover mask, bias in trees outside the NFI forest definition, which NFI plots do not sample.

These estimated quantities could be used to correct the maps but we have opted not to do so, for two reasons. First, the NFI plots are only measured in areas meeting the NFI forest definition (which is independent of the land-cover map) and do not systematically cover trees outside forest; however, the tree-cover mask includes tree cover outside forest, such as hedgerows and groups of trees below the NFI size threshold. Thus, for the tree-cover mask

any correction would be an extrapolation rather than an estimate grounded on field data. Second, correcting only the forest mask would make the totals inconsistent, so the difference between them would no longer be meaningful for distinguishing between forest biomass and biomass in trees outside forest. In any case, on the held-out plots the corrections are not significantly different from zero, and applying them would not move stocks and stock changes beyond their confidence intervals (Table 1).

Comparisons with other products and local references

We benchmarked our model against available biomass and canopy-height products with coverage over Denmark (Extended Data Table 1). As the products differed in resolution and coordinate reference system (CRS), we transformed Danish plot and site geometries into each product's own CRS without resampling or warping. For NFI plot-level sampling, we took the mean of every pixel whose footprint intersected the 15 m plot radius: each candidate pixel's corners were reprojected individually into EPSG:25832, and the pixel was included when any part of the resulting quadrilateral lay within 15 m of the NFI plot centre. Distances were measured in EPSG:25832, so the sampled area is a true 15 m circle on the ground; applying a fixed angular radius to the products distributed in EPSG:4326 would instead have described an ellipse, elongated north–south by a factor of 1.7–1.9 across Danish latitudes. Using overlap as a criterion is necessary at varying resolutions, as a 100 m pixel centre may not fall within 15 m of an NFI plot centre, even if the plot is wholly contained by the pixel. Projecting the corners individually is relevant when the product's own grid is rotated relative to UTM zone 32N, as in the ICESat-2 Albers grid which is rotated by 35–45° at Danish longitudes. Taking the footprint means rather than single-pixel values avoids single-pixel noise when pixel size is smaller than plot size, and allows for inclusion of overlapping pixels. Pixel values of 0 were treated as predicted biomass or canopy height of 0 and were included; only pixels carrying a product's fill value (indicating no prediction for that pixel) were excluded. For the plot-level benchmark we used the test plots measured in 2019–2020, the years lying within one year of every product's reference year (Extended Data Table 1). Each benchmark was sampled at its reference year (2020 for FCM), except ESA-CCI, which has a map for every year and was sampled at each plot's measurement year; our model was sampled from the 2019–2023 composite, whose scan at each test plot lies within one year of the field measurement.

For forest-level comparisons in our reference areas (the managed Frederiksdal estate and the Suserup reserve), we followed the same native-resolution principle as above for all the products, but aggregated over site boundaries rather than plot footprints. At Suserup, field measurements used in this study were taken in 2013 and 2023 and biomass estimated for each tree according to the procedure described in Nord-Larsen et al. [75]. We create a boundary at Suserup by applying a concave hull (max. edge length ratio = 0.3) around the geolocated individual tree stem locations, with a 20 m buffer. In Frederiksdal, we used the stand-level polygons only using managed stands where the sample-plot based field inventory (15 m plots as in the NFI, collected in 2015 and 2025) was taken, covering 148 ha of the estate's $\approx$ 200 ha of forest. As with the plot comparison, for biomass we took the mean of pixels within the boundaries. Since coarse pixels may lie only partly inside a boundary, we apply a weighted mean for pixels with only partial overlap; each pixel is weighted according to the fraction of its area inside the boundary. A binary pixel in-or-out test based on pixel centres could disfavour the combination of coarse pixels and smaller areas; by area-weighting we are able to give the same footprint to products with different native resolutions. To avoid penalising products for their own mask, pixels having no data within a boundary are not treated as 0 biomass but are removed and the weights renormalised.

Canopy height was analysed differently as for each pixel it is a maximum quantity rather than a rate-per-ha, as was the case for biomass. We took the mean value of the model hexagons within the boundaries (for field reference, we take the highest measured tree within each hexagon at Suserup, and area-weighted stand height at Frederiksdal); for the benchmarks, we took the maximum of the pixels whose centres fall within each hexagon, then the mean of those per-hexagon maxima. Where a height product publishes a per-pixel standard deviation we take the per-hexagon mean instead of the maximum; if we took the max it would identify the noisiest pixel in the window as opposed to the noise associated with the hexagon. In Figure 3 we show published product uncertainties, which should not be confused with area-based confidence intervals: for our model it is the mean Q25-Q75 interval and for other products it is the mean pixel standard deviation.

Evaluation of canopy height as a biomass proxy over space and time

We conducted this analysis on two different sets of data: the model-independent NFI field measurements collected over two decades, and the national predictions from our model. We also use local field inventory in our managed forest reference (Frederiksdal) where we have temporal overlap with LiDAR scans.

For the field analysis, we used the longitudinal series of the permanent plots in the Danish NFI to characterise the height-biomass relationship cross-sectionally and over time. The plots are remeasured every 5 years, meaning a single plot may appear up to 5 times with corresponding canopy height measurements and biomass estimations. There are 9,469 measurement instances over 2,650 plots, with 7,250 paired remeasurements. We then compared two quantities, the correlation between height and biomass across plots ($r = 0.77$), and the correlation between Δh_{can} and ΔAGB within a plot over time ($r = 0.51$). The first statistic represents between-stand variation (taller forests do correlate with higher biomass) and the second represents local change. Using Spearman's ranks, the contrast is stronger: $\rho = 0.83$ between plots against $\rho = 0.33$ within them. Where biomass declined by more than 2 Mg ha^{-1} between paired measurements, we considered canopy height to be stable or increasing when $\Delta h_{\text{can}} \geq -0.5$ m; this applied to 57.8% of the pairs.

For the model outputs, over the 21,929,039 hexagons with predictions in both composites we categorised each pair by modelled biomass change (a decline being $\Delta\text{AGB} < -2$ Mg ha^{-1}) and by modelled height change: rising height ($\Delta h_{\text{can}} > +0.5$ m), stable height ($|\Delta h_{\text{can}}| \leq 0.5$ m) and falling height ($\Delta h_{\text{can}} < -0.5$ m). The criteria are therefore the same as applied to the field pairs. The fractions of hexagons with diverging height and biomass are reported over the forest mask (classes 13 and 14 of the 2021 land cover, 10,730,911 hexagons); the tree-cover mask gives 63.5% in place of 64.6%. Basal area was taken from the same model output. Because the map interval varies with scan campaign, the effective gap between composites ranges from five to nine years by location, against exactly five years for the field pairs, so the two fractions are similar but not measured over identical intervals. This divergence between height and biomass illustrates that while the model outputs are derived from the same learned representation of the point cloud, the model does not derive biomass from a monotone function of height.

At Frederiksdal we use the example of stand 45_a (see Fig. 4), one of the larger stands at the estate and where there was a known thinning carried out in the winter of 2022–23. Stand-level values are the mean over hexagon centroids falling within the stand polygon, as for the other Frederiksdal stands, and it is covered by three national LiDAR scans in five-year intervals (2014, 2019, 2024). The stand-level statistic over Frederiksdal uses the stricter criterion $\Delta\text{AGB} < 0$ with $\Delta h_{\text{can}} \geq 0$, over the 183.1 ha of forest stands carrying model predictions in both 2019 and 2024. Compartments recorded as non-forest land use such as agricultural land, buildings, roads, and water bodies are excluded.

Acknowledgements. The authors would like to acknowledge all of the people who collected the measurement data for the forest inventory, and wish to thank Siyu Liu for making available the high-resolution version of the canopy-height map.

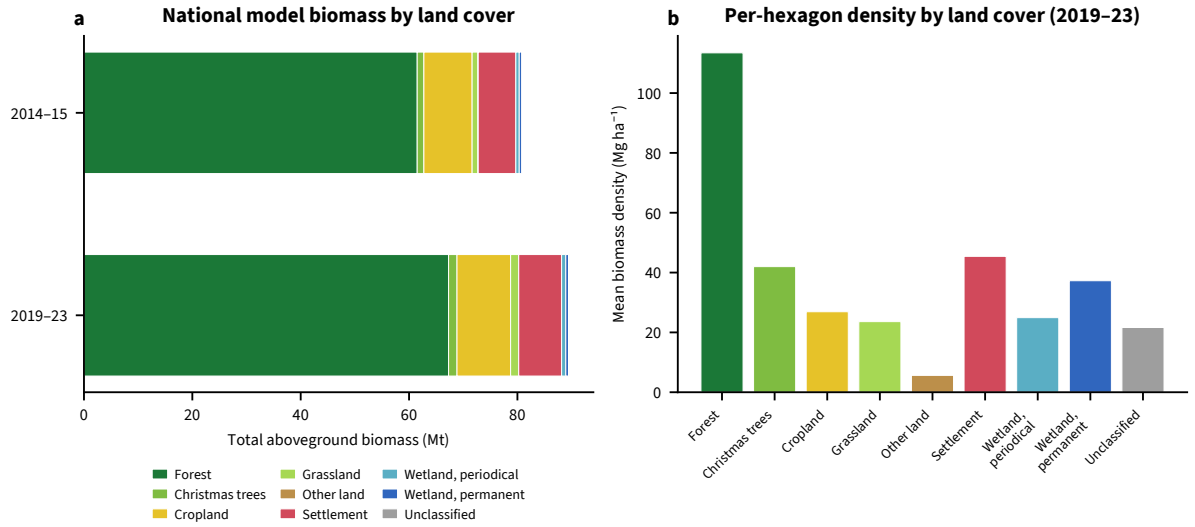
Declarations

- **Funding**:
  H.B. declares funding support for this work from The Danish Agricultural Agency (Grant number 33010-NIFA-22-845: "The impact of forest management on carbon stocks and the resulting climate effects").
  T.N-L. declares funding support from the LIFE Programme of the European Union through the project "Forest fit for future" (LIFE4Forest, LIFE19 ENV/DK/000013). Views and opinions expressed are however those of the authors only and do not necessarily reflect those of the European Union or the European Climate, Infrastructure and Environment Executive Agency (CINEA). Neither the European Union nor the granting authority can be held responsible for them.
  C.I. declares funding support from the Danish National Research Foundation through the Center of Excellence "Remote Sensing and Deep Learning of Global Tree Resources" (TreeSense, DNRF192).
- **Competing interests**
  The authors declare no competing interests.
- **Data availability**
  The time series of forest maps produced with this study are available on Zenodo: https://doi.org/10.5281/zenodo.22283051. The national airborne LiDAR point clouds [70], surface and terrain models [41, 42] and orthophotos [31] are publicly available from Klimadatastyrelsen, and the benchmark products from the sources cited in Extended Data Table 1, except the native-resolution canopy-height layer of Liu et al., which was provided by the authors. The land-use/land-cover maps were provided by the Danish Centre for Environment and Energy, Aarhus University [32], and are available from the Centre on request. Source data for Figs. 2, 3, 4 and 6 and Extended Data Figs. 1 and 4 and Extended Data Table 3 will be provided with the published paper. The Danish field reference data (NFI, Suserup, and Frederiksdal) is not public but is available by data-sharing agreement with Thomas Nord-Larsen: tnl@ign.ku.dk.
- **Code availability**

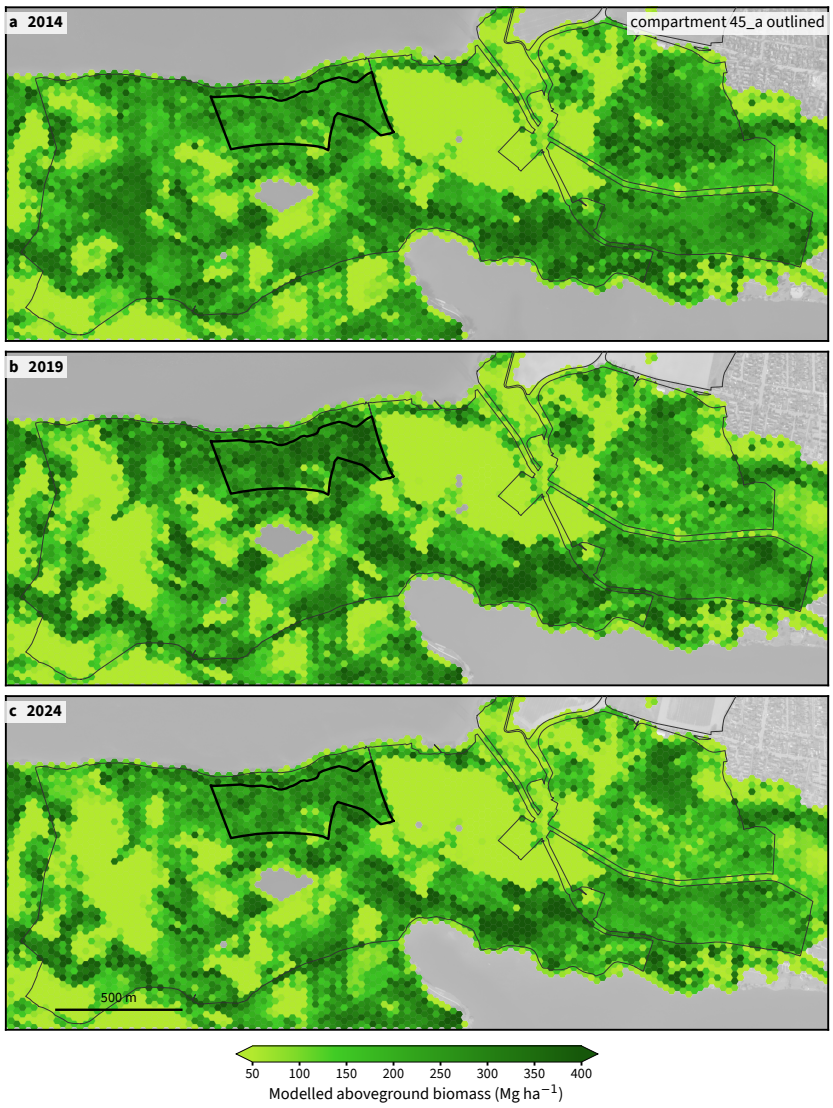
The code that builds the maps from the model predictions and produces the numbers, figures, and tables in the manuscript, the model code and the model weights will be made publicly available upon publication.

- **Author contribution**
  H.B., S.O., T.N-L., and C.I. conceived the design of the study; H.B. and T.N-L. participated in field data collection. S.O. and H.B. developed model code, and H.B. trained the model, produced the maps, and conducted the analysis under the supervision of S.O., T.N-L., and C.I. All authors contributed to drafting and editing the final manuscript.

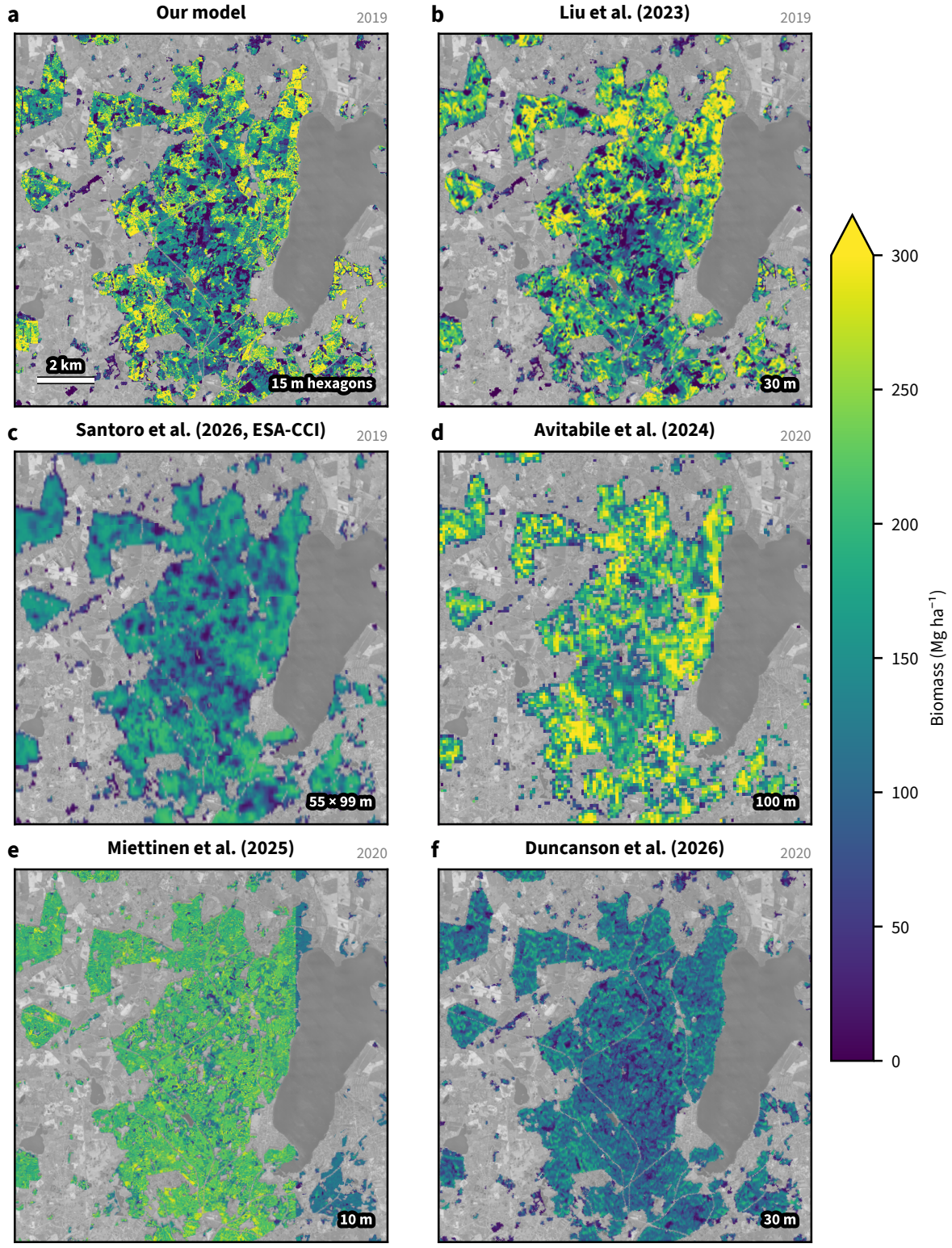
Extended data



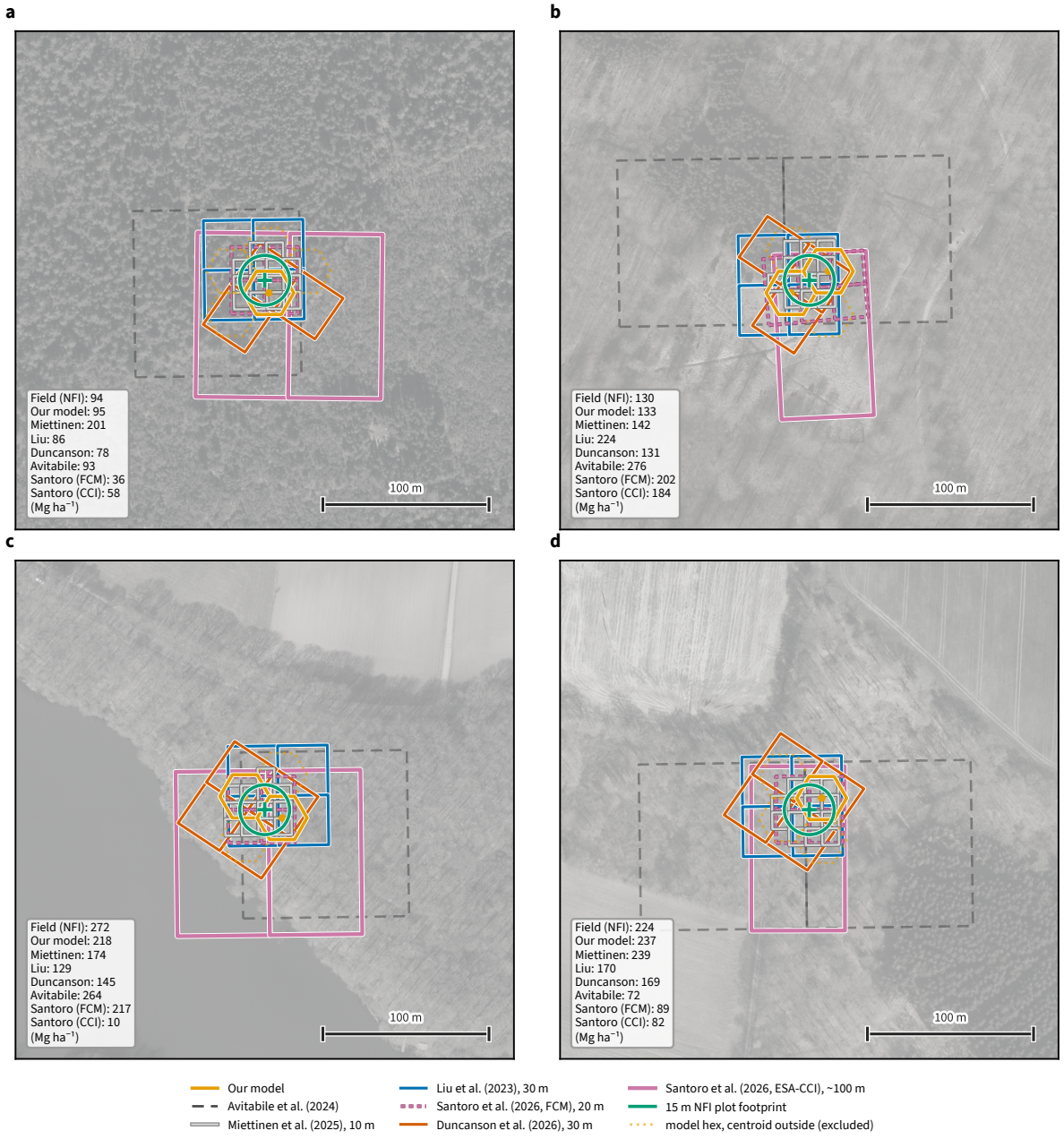
Extended Data Fig. 1: **Biomass and per hexagon biomass density by land-cover type.** Panel **a** shows total aboveground biomass over different land-cover types under the tree-cover mask. In **b** it can be seen that land-cover pixels classified as forest tend to have higher densities than in other land-cover types. Classes are the IPCC land-use categories as mapped in the Danish national land-use/land-cover maps used for UNFCCC reporting [32], except that Christmas-tree plantations are reported separately from the rest of the forest category.



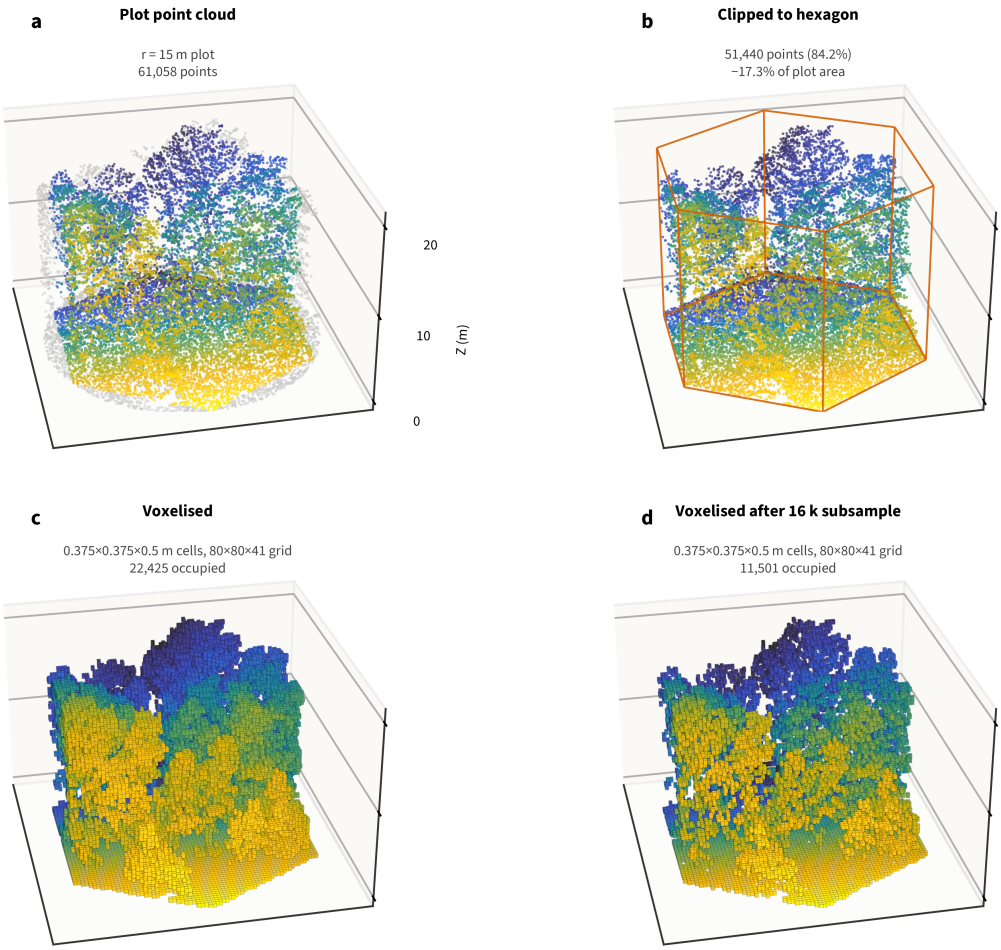
Extended Data Fig. 2: **Modelled aboveground biomass across the managed reference forest (Frederiksdal). a–c**, model predictions at native hexagon resolution in the site's scan years (2014, 2019, 2024), on the colour scale of Fig. 4. Forest boundaries are outlined with compartment 45_a, shown in Fig. 4, in bold. Orthophoto basemaps contain data from Klimadatastyrelsen, GeoDanmark spring orthophotos [31].



Extended Data Fig. 3: **Fig. 5 at product-native resolution.** The landscape of Fig. 5 (approx. 13 × 13 km) with each product on its own grid instead of aggregated to 100 m: **a** our model (15 m circumradius hexagons), **b** Liu et al. [35] (30 m), **c** Santoro et al. [33] (ESA-CCI; 1/1125° cells, 55 × 99 m at this latitude), **d** Avitabile et al. [36] (100 m), **e** Miettinen et al. [37] (10 m; the step towards the right is where Sentinel-2 tiles join), **f** Duncanson et al. [19] (30 m, on a grid rotated relative to the map). Cells are shown where their centre falls within the forest hexagons of **a**. Colour scale as in Fig. 5; values above 300 Mg ha^{-1} are more frequent than there because native cells are not averaged. Orthophoto: Klimadatastyrelsen [31].



Extended Data Fig. 4: **Sampling geometries of different models.** Panels **a**–**d** represent actual sampling geometries of benchmark products, the field NFI reference plot, and the model. For benchmark products, pixels having a boundary within 15 m of plot centre are averaged, while model predictions with centre points within 15 m are averaged. **a** and **b** represent plots in contiguous forest areas while **c** and **d** highlight potential edge effects of coarser resolution products.



Extended Data Fig. 5: **Availability of forest structure to the model.** Panel **a** is an example of an NFI plot point cloud; points in grey will be removed after clipping to hexagonal shape; **b** the point cloud clipped; **c** the clipped cloud voxelised; and **d** the voxelised point cloud after downsampling to ($n = 16{,}000$). The number of voxels is less than the number of points due to pooling when more than one point would have occupied the grid.

Extended Data Table 1: **Benchmark products.** Nominal resolution is listed for each product, though pixels for products using EPSG:4326 CRS are not square at Danish latitudes. These pixels are elongated north–south; the nominal 100 m ESA-CCI pixel (Santoro et al. (ESA-CCI)), for example, measures approximately 57 m east–west by 99 m north–south at 55°N. Reference year is the nominal year each product represents, used for temporal matching (Methods); where a product is built from a multi-year image mosaic the acquisition window is given in parentheses. The acquisition year of the Danish DHM nDSM tile used here is approximate. The Liu et al. canopy-height layer is obtained from the authors' native-resolution product; the publicly available version is aggregated to 30 m. Liu et al. biomass is in kg pixel^{-1}, all other biomass products in Mg ha^{-1}, and all canopy heights in m.

Product (CRS)	Resolution	EO data	Retrieval method	Reference year
Aboveground biomass				
Liu et al. [35] EPSG:3035	30 m	PlanetScope (optical)	Deep learning for canopy height (ALS labels) and tree cover; power law per forest type, calibrated on 11,296 Danish NFI plots	2019
Santoro et al. (ESA-CCI) [33] EPSG:4326	100 m	Sentinel-1 (C-band) and ALOS-2 PALSAR-2 (L-band) synthetic aperture radar (SAR)	BIOMASAR water-cloud model; LiDAR-trained structural functions, height–AGB law fitted to sub-national and FAO inventory statistics	2015–2024 (annual)
Santoro et al. (FCM) [34] EPSG:32632/32633 (UTM, per Sentinel-2 tile)	20 m	Sentinel-1 (C-band) and ALOS-2 PALSAR-2 (L-band) SAR	BIOMASAR as above, but height–GSV law fitted per European ecoregion to provincial inventory statistics; AGB derived with leaf-type-specific allometry	2017, 2020, 2021, 2023
Avitabile et al. [36] EPSG:3035	100 m	ESA-CCI 2020 (SAR)	Rescaled per administrative unit to harmonised inventory statistics	2020
Duncanson et al. [19] Custom Albers equal-area	30 m	ICESat-2 ATL08 LiDAR and HLS optical	Field-trained model on ICESat-2 height metrics; random-forest extrapolation on spectral and topographic covariates	2020
Miettinen et al. [37] EPSG:3035	10 m	Sentinel-2 mosaic	k-NN ($k = 7$) from ≈151,000 NFI plots (none in Denmark); Copernicus forest-type and tree-cover-density layers	2020
Canopy height				
Liu et al. [35] EPSG:4326	≈3 m	PlanetScope (optical)	Deep learning on ALS labels; GEDI/Sentinel-2 height map as auxiliary input	2019
Lang et al. [38] EPSG:4326	10 m	Sentinel-2	Deep learning, GEDI-trained	2020
Tolan et al. [39] EPSG:3857	1 m	Maxar Vivid2 mosaic	Self-supervised ViT and dense decoder trained on aerial LiDAR; GEDI-trained correction CNN	2020 (2017–2020)
Brandt et al. [40] EPSG:3857	1 m	Maxar Vivid2 mosaic	DINOv3 depth model trained on ALS; GEDI/ICESat-2 for validation only	2020 (2017–2020)
DHM nDSM [41, 42] EPSG:25832	0.4 m	Airborne LiDAR (ALS)	Surface model minus terrain model	≈2019

Extended Data Table 2: **Model test-set performance.** Accuracy on $n = 735$ NFI plots held out from training, model selection, and calibration evaluated against field measurements. Metrics are computed on the bias-corrected predictions (the values used for the national maps); R^2 and RMSE are identical on the raw predictions to within 0.002 and 0.1 unit, respectively (Extended Data Table 3). Plots where field-measured canopy height and a model-independent LiDAR height metric (95th − 5th percentile of return elevations) disagreed by more than 10 m (which suggest disturbance between field inventory and scan) were excluded as label/scan mismatches, the same model-independent criterion applied in Table 2; the full $n = 764$ set is reported in Extended Data Table 3. RMSE and MAE are in each attribute's native unit; rRMSE is RMSE as a percentage of the field mean. Bias is the mean signed error (prediction minus ground truth) remaining after the train/validation median bias correction. Values in parentheses are 95% confidence intervals from a 10,000-iteration bootstrap; they reflect test-plot sampling variability only and do not account for any measurement/allometric error.

Attribute	n	R^2	RMSE	rRMSE (%)	MAE	Bias (95% CI)
AGB (Mg ha^{-1})	735	0.85	39.4	34.6	26.6	−2.7 (−5.8, 0.3)
Stem volume (m^3 ha^{-1})	735	0.85	72.8	34.0	48.8	−4.9 (−10.6, 0.7)
Canopy height (m)	735	0.93	2.39	13.0	1.65	0.19 (0.01, 0.37)
Basal area (m^2 ha^{-1})	735	0.77	6.17	31.1	4.51	−0.51 (−1.00, −0.04)

Extended Data Table 3: **Sensitivity of held-out test performance to the two post-hoc operations.** Effect of the median bias correction and of excluding label/scan-mismatch plots ($|h_{\text{can}}^{\text{field}} - h_{\text{can}}^{\text{LiDAR}}| > 10$ m) on held-out test R^2 and RMSE ($n = 764$ before exclusion, 735 after). Bias correction changes R^2 by < 0.002 and RMSE by < 0.1 unit for every attribute; note that it removes an aggregate offset for national sums, not per-plot error. Excluding the 29 mismatch plots (3.8%) raises R^2 by 0.02–0.06, most for canopy height because the exclusion criterion is height-based. Extended Data Table 2 reports the bias-corrected, QC-filtered column.

		Unfiltered ($n = 764$)		QC-filtered ($n = 735$)	
Attribute	metric	raw	corrected	raw	corrected
Aboveground biomass	R^2	0.831	0.831	0.849	0.849
	RMSE	42.79	42.75	39.47	39.43
Stem volume	R^2	0.822	0.822	0.853	0.853
	RMSE	81.86	81.92	72.71	72.76
Canopy height	R^2	0.868	0.869	0.928	0.929
	RMSE	3.37	3.36	2.41	2.39
Basal area	R^2	0.730	0.730	0.771	0.772
	RMSE	6.80	6.79	6.18	6.17

References

[1] Pan, Y. *et al.* A Large and Persistent Carbon Sink in the World's Forests. *Science* **333**, 988–993 (2011). URL https://www.science.org/doi/full/10.1126/science.1201609.

[2] Pan, Y. *et al.* The enduring world forest carbon sink. *Nature* **631**, 563–569 (2024). URL https://www.nature.com/articles/s41586-024-07602-x.

[3] Harris, N. L. *et al.* Global maps of twenty-first century forest carbon fluxes. *Nature Climate Change* **11**, 234–240 (2021). URL https://doi.org/10.1038/s41558-020-00976-6.

[4] Grassi, G. *et al.* The key role of forests in meeting climate targets requires science for credible mitigation. *Nature Climate Change* **7**, 220–226 (2017). URL https://www.nature.com/articles/nclimate3227.

[5] IPCC. 2019 Refinement to the 2006 IPCC Guidelines for National Greenhouse Gas Inventories, Volume 4: Agriculture, Forestry and Other Land Use. Tech. Rep., Intergovernmental Panel on Climate Change (2019).

[6] European Parliament and Council of the European Union. Regulation (EU) 2018/841 of the European Parliament and of the Council of 30 May 2018 on the inclusion of greenhouse gas emissions and removals from land use, land use change and forestry in the 2030 climate and energy framework. Official Journal of the European Union, L 156, 19.6.2018, p. 1–25 (2018).

[7] European Parliament and Council of the European Union. Regulation (EU) 2023/839 of the European Parliament and of the Council of 19 April 2023 amending Regulation (EU) 2018/841 as regards the scope, simplifying the compliance rules, setting out the targets of the Member States for 2030 and committing to the collective achievement of climate neutrality by 2035 in the land use, forestry and agriculture sector. Official Journal of the European Union, L 107, 26.4.2023, p. 1–28 (2023).

[8] FAO. *Global Forest Resources Assessment 2025* (FAO, Rome, Italy, 2025). URL https://openknowledge.fao.org/handle/20.500.14283/cd6709en.

[9] Badgley, G. *et al.* Systematic over-crediting in California's forest carbon offsets program. *Global Change Biology* **28**, 1433–1445 (2022). URL https://onlinelibrary.wiley.com/doi/abs/10.1111/gcb.15943.

[10] West, T. A. P. *et al.* Action needed to make carbon offsets from forest conservation work for climate change mitigation. *Science* **381**, 873–877 (2023). URL https://www.science.org/doi/10.1126/science.ade3535.

[11] Romm, J., Lezak, S. & Alshamsi, A. Are Carbon Offsets Fixable? *Annual Review of Environment and Resources* **50**, 649–680 (2025). URL https://www.annualreviews.org/content/journals/10.1146/annurev-environ-112823-064813.

[12] Anderson, C. B. *et al.* Forest Carbon Diligence: Digital MRV for mapping forest structure and carbon stocks. *Forest Ecology and Management* **612**, 123709 (2026). URL https://www.sciencedirect.com/science/article/pii/S0378112726002070.

[13] Mitchard, E. T. *et al.* Uncertainty in the spatial distribution of tropical forest biomass: a comparison of pan-tropical maps. *Carbon Balance and Management* **8**, 10 (2013). URL https://doi.org/10.1186/1750-0680-8-10.

[14] Araza, A. *et al.* A comprehensive framework for assessing the accuracy and uncertainty of global above-ground biomass maps. *Remote Sensing of Environment* **272**, 112917 (2022). URL https://www.sciencedirect.com/science/article/pii/S0034425722000311.

[15] Santoro, M. *et al.* Design and performance of the Climate Change Initiative Biomass global retrieval algorithm. *Science of Remote Sensing* **10**, 100169 (2024). URL https://www.sciencedirect.com/science/article/pii/S2666017224000531.

[16] Dubayah, R. *et al.* The Global Ecosystem Dynamics Investigation: High-resolution laser ranging of the Earth's forests and topography. *Science of Remote Sensing* **1**, 100002 (2020). URL https://www.

sciencedirect.com/science/article/pii/S2666017220300018.

[17] Dubayah, R. *et al.* GEDI launches a new era of biomass inference from space. *Environmental Research Letters* **17**, 095001 (2022). URL https://doi.org/10.1088/1748-9326/ac8694.

[18] Duncanson, L. *et al.* Aboveground biomass density models for NASA's Global Ecosystem Dynamics Investigation (GEDI) lidar mission. *Remote Sensing of Environment* **270**, 112845 (2022). URL https://www.sciencedirect.com/science/article/pii/S0034425721005654.

[19] Duncanson, L. *et al.* Global and boreal estimates of woody aboveground biomass for 2020: Filling GEDI's northern data gap with ICESat-2 and Harmonized Landsat Sentinel-2. *Remote Sensing of Environment* **340**, 115406 (2026). URL https://www.sciencedirect.com/science/article/pii/S0034425726001768.

[20] White, J. C. *et al.* Remote Sensing Technologies for Enhancing Forest Inventories: A Review. *Canadian Journal of Remote Sensing* **42**, 619–641 (2016). URL https://doi.org/10.1080/07038992.2016.1207484.

[21] Næsset, E. Predicting forest stand characteristics with airborne scanning laser using a practical two-stage procedure and field data. *Remote Sensing of Environment* **80**, 88–99 (2002). URL https://www.sciencedirect.com/science/article/pii/S0034425701002905.

[22] Nilsson, M. *et al.* A nationwide forest attribute map of Sweden predicted using airborne laser scanning data and field data from the National Forest Inventory. *Remote Sensing of Environment* **194**, 447–454 (2017). URL https://www.sciencedirect.com/science/article/pii/S0034425716303947.

[23] Hauglin, M., Rahlf, J., Schumacher, J., Astrup, R. & Breidenbach, J. Large scale mapping of forest attributes using heterogeneous sets of airborne laser scanning and National Forest Inventory data. *Forest Ecosystems* **8**, 65 (2021). URL https://doi.org/10.1186/s40663-021-00338-4.

[24] Nord-Larsen, T. & Schumacher, J. Estimation of forest resources from a country wide laser scanning survey and national forest inventory data. *Remote Sensing of Environment* **119**, 148–157 (2012). URL https://www.sciencedirect.com/science/article/pii/S0034425712000107.

[25] Magnussen, S., Nord-Larsen, T. & Riis-Nielsen, T. Lidar supported estimators of wood volume and aboveground biomass from the Danish national forest inventory (2012–2016). *Remote Sensing of Environment* **211**, 146–153 (2018). URL https://www.sciencedirect.com/science/article/pii/S0034425718301615.

[26] Nord-Larsen, T. & Johannsen, V. K. Danish National Forest Inventory: Design and calculations. Report 978-87-7903-746-5, Department of Geosciences and Natural Resource Management, University of Copenhagen (2016).

[27] Oehmcke, S. *et al.* Deep point cloud regression for above-ground forest biomass estimation from airborne LiDAR. *Remote Sensing of Environment* **302**, 113968 (2024). URL https://www.sciencedirect.com/science/article/pii/S0034425723005205.

[28] Koenker, R. & Bassett, G., Jr. Regression quantiles. *Econometrica* **46**, 33–50 (1978).

[29] Taylor, J. W. A quantile regression neural network approach to estimating the conditional density of multiperiod returns. *Journal of Forecasting* **19**, 299–311 (2000).

[30] Steinwart, I. & Christmann, A. Estimating conditional quantiles with the help of the pinball loss. *Bernoulli* **17**, 211–225 (2011). URL https://doi.org/10.3150/10-BEJ267.

[31] Klimadatastyrelsen. GeoDanmark ortofoto, forår. Dataforsyningen, WMS service. URL https://api.dataforsyningen.dk/orto_foraar_DAF.

[32] Levin, G. & Gyldenkærne, S. Estimating land use/land cover and changes in Denmark: technical documentation for the assessment of annual land use/land cover and changes since 2011. Tech. Rep. 227, Aarhus University, DCE – Danish Centre for Environment and Energy, Aarhus, Denmark (2022). URL https://dce2.au.dk/pub/TR227.pdf.

[33] Santoro, M. & Cartus, O. ESA Biomass Climate Change Initiative (Biomass_cci): Global datasets of forest above-ground biomass for the years 2005-2012 and 2015-2024, v7.0 (2026). URL https://catalogue.ceda.ac.uk/uuid/6429d1aafe1e43b9b414e4a5a7f8b903.

[34] Santoro, M. *et al.* Europe-wide maps of biomass density based on satellite remote sensing data for 2017, 2020, 2021 and 2023. *Data in Brief* **65**, 112536 (2026).

[35] Liu, S. *et al.* The overlooked contribution of trees outside forests to tree cover and woody biomass across Europe. *Science Advances* **9**, eadh4097 (2023). URL https://doi.org/10.1126/sciadv.adh4097.

[36] Avitabile, V. *et al.* Harmonised statistics and maps of forest biomass and increment in Europe. *Scientific Data* **11**, 274 (2024). URL https://www.nature.com/articles/s41597-023-02868-8.

[37] Miettinen, J. *et al.* Pan-European forest maps produced with a combination of earth observation data and national forest inventory plots. *Data in Brief* **60**, 111613 (2025). URL https://www.sciencedirect.com/science/article/pii/S2352340925003452.

[38] Lang, N., Jetz, W., Schindler, K. & Wegner, J. D. A high-resolution canopy height model of the Earth. *Nature Ecology & Evolution* **7**, 1778–1789 (2023). URL https://doi.org/10.1038/s41559-023-02206-6.

[39] Tolan, J. *et al.* Very high resolution canopy height maps from RGB imagery using self-supervised vision transformer and convolutional decoder trained on aerial lidar. *Remote Sensing of Environment* **300**, 113888 (2024). URL https://www.sciencedirect.com/science/article/pii/S003442572300439X.

[40] Brandt, J. *et al.* CHMv2: Improvements in Global Canopy Height Mapping using DINOv3 (2026). URL http://arxiv.org/abs/2603.06382. ArXiv:2603.06382 [cs.CV].

[41] Klimadatastyrelsen. Danmarks Højdemodel – Overflade. Dataforsyningen (2026). URL https://dataforsyningen.dk/data/928.

[42] Klimadatastyrelsen. Danmarks Højdemodel – Terræn. Dataforsyningen (2026). URL https://dataforsyningen.dk/data/930.

[43] Nord-Larsen, T. *et al.* Skovstatistik 2023. Report, Department of Geosciences and Natural Resource Management, University of Copenhagen, Frederiksberg (2024). URL https://curis.ku.dk/ws/portalfiles/portal/447618920/Rapport_Skovstatistik_2023_web.pdf. In Danish.

[44] Santoro, M. & Cartus, O. CCI Biomass Product User Guide, Version 7.0. Tech. Rep. D4.3-PUG, Aberystwyth University and GAMMA Remote Sensing (2026). URL https://climate.esa.int/documents/3352/Product_User_Guide_PUG_V7.0.pdf. Issue 7.0, 19 March 2026.

[45] Santoro, M., Cartus, O., Lucas, R. & Friendship-Kay, H. CCI Biomass Algorithm Theoretical Basis Document, Version 7.0. Tech. Rep. D2.2-ATBD, Aberystwyth University and GAMMA Remote Sensing (2025). URL https://climate.esa.int/documents/3351/Algorithm_Theoretical_Basis_Document_ATBD_V7.0.pdf. Issue 7.0, 17 December 2025.

[46] Wheeler, C. E. *et al.* The path to robust evaluation of carbon credits generated by forest restoration and REDD+ projects. *Remote Sensing of Environment* **332**, 115041 (2026). URL https://www.sciencedirect.com/science/article/pii/S0034425725004456.

[47] Van Winckel, S., Simons, J., Lhermitte, S. & Muys, B. Assessing the effect of forest management on above-ground carbon stock by remote sensing. *Biogeosciences* **22**, 4291–4307 (2025). URL https://bg.copernicus.org/articles/22/4291/2025/.

[48] Zhang, H. *et al.* A vertical vegetation structure model of the Earth (2026). URL https://eartharxiv.org/repository/view/15380/.

[49] Lesiv, M. *et al.* Global forest management data for 2015 at a 100 m resolution. *Scientific Data* **9**, 199 (2022). URL https://www.nature.com/articles/s41597-022-01332-3.

[50] FOREST EUROPE. State of Europe's Forests 2025. Tech. Rep., FOREST EUROPE Liaison Unit Sweden, Stockholm, Sweden (2026). URL https://foresteurope.org/wp-content/uploads/2026/03/SoEF_2025_updated-version-May-2026.pdf.

[51] Hansen, M. C. *et al.* High-Resolution Global Maps of 21st-Century Forest Cover Change. *Science* **342**, 850–853 (2013). URL https://www.science.org/doi/10.1126/science.1244693.

[52] Asner, G. P., Rudel, T. K., Aide, T. M., Defries, R. & Emerson, R. A Contemporary Assessment of Change in Humid Tropical Forests. *Conservation Biology* **23**, 1386–1395 (2009). URL https://onlinelibrary.wiley.com/doi/abs/10.1111/j.1523-1739.2009.01333.x.

[53] Berenguer, E. *et al.* A large-scale field assessment of carbon stocks in human-modified tropical forests. *Global Change Biology* **20**, 3713–3726 (2014). URL https://onlinelibrary.wiley.com/doi/abs/10.1111/gcb.12627.

[54] Heinrich, V. *et al.* A meta-analysis of carbon losses and gains from tropical moist forest degradation and regeneration. *Science Advances* **12**, eadz1923 (2026). URL https://www.science.org/doi/abs/10.1126/sciadv.adz1923.

[55] Radeloff, V. C. *et al.* Need and vision for global medium-resolution Landsat and Sentinel-2 data products. *Remote Sensing of Environment* **300**, 113918 (2024). URL https://www.sciencedirect.com/science/article/pii/S0034425723004704.

[56] van der Woude, S. *et al.* European forest disturbance alerting using Sentinel-1. *Remote Sensing of Environment* **337**, 115325 (2026). URL https://www.sciencedirect.com/science/article/pii/S0034425726000957.

[57] Schwartz, M. *et al.* FORMSpoT: Revealing fine-scale forest disturbances from nation-wide 1.5 m forest canopy height time series. *Remote Sensing of Environment* **346**, 115631 (2026). URL https://www.sciencedirect.com/science/article/pii/S0034425726004013.

[58] Boser, A. Validating spatio-temporal environmental machine learning models: Simpson's paradox and data splits. *Environmental Research Communications* **6**, 031003 (2024). URL https://doi.org/10.1088/2515-7620/ad2e44.

[59] Damgaard, C. A Critique of the Space-for-Time Substitution Practice in Community Ecology. *Trends in Ecology & Evolution* **34**, 416–421 (2019). URL https://www.sciencedirect.com/science/article/pii/S016953471930028X.

[60] Kreyling, J. Space-for-time substitution misleads projections of plant community and stand-structure development after disturbance in a slow-growing environment. *Journal of Ecology* **113**, 68–80 (2025). URL https://onlinelibrary.wiley.com/doi/abs/10.1111/1365-2745.14438.

[61] Evans, M. E. K. *et al.* Reconsidering space-for-time substitution in climate change ecology. *Nature Climate Change* **15**, 809–812 (2025). URL https://www.nature.com/articles/s41558-025-02392-0.

[62] Kennedy, R. E., Yang, Z. & Cohen, W. B. Detecting trends in forest disturbance and recovery using yearly Landsat time series: 1. LandTrendr — Temporal segmentation algorithms. *Remote Sensing of Environment* **114**, 2897–2910 (2010). URL https://www.sciencedirect.com/science/article/pii/S0034425710002245.

[63] Sanders-DeMott, R. *et al.* Ground-Truth: Can Forest Carbon Protocols Ensure High-Quality Credits? *Earth's Future* **13**, e2024EF005414 (2025). URL https://onlinelibrary.wiley.com/doi/abs/10.1029/2024EF005414.

[64] Forster, E. J., Healey, J. R., Dymond, C. & Styles, D. Commercial afforestation can deliver effective climate change mitigation under multiple decarbonisation pathways. *Nature Communications* **12**, 3831 (2021). URL https://www.nature.com/articles/s41467-021-24084-x.

[65] Deng, X. *et al.* Forest biodiversity increases productivity via complementarity from greater canopy structural complexity. *Proceedings of the National Academy of Sciences* **122**, e2506750122 (2025). URL https://www.pnas.org/doi/abs/10.1073/pnas.2506750122.

[66] Ehbrecht, M. *et al.* Global patterns and climatic controls of forest structural complexity. *Nature Communications* **12**, 519 (2021). URL https://www.nature.com/articles/s41467-020-20767-z.

[67] Marvin, D. C. *et al.* Amazonian landscapes and the bias in field studies of forest structure and biomass. *Proceedings of the National Academy of Sciences* **111**, E5224–E5232 (2014). URL https://www.pnas.org/doi/full/10.1073/pnas.1412999111.

[68] Labrière, N. *et al.* Toward a forest biomass reference measurement system for remote sensing applications. *Global Change Biology* **29**, 827–840 (2023). URL https://onlinelibrary.wiley.com/doi/abs/10.1111/gcb.16497.

[69] Fischer, F. J. *et al.* The Global Canopy Atlas: analysis-ready maps of 3D structure for the world's woody ecosystems (2025). URL https://www.biorxiv.org/content/10.1101/2025.08.31.673375v2.

[70] Klimadatastyrelsen. Danmarks Højdemodel – Punktsky. Dataforsyningen. URL https://dataforsyningen.dk/data/3931.

[71] Choy, C., Gwak, J. & Savarese, S. 4D spatio-temporal ConvNets: Minkowski convolutional neural networks. *Proc. IEEE/CVF Conference on Computer Vision and Pattern Recognition (CVPR)* 3075–3084 (2019). URL https://openaccess.thecvf.com/content_CVPR_2019/html/Choy_4D_Spatio-Temporal_ConvNets_Minkowski_Convolutional_Neural_Networks_CVPR_2019_paper.html.

[72] Huber, P. J. Robust estimation of a location parameter. *The Annals of Mathematical Statistics* **35**, 73–101 (1964).

[73] Igel, C. & Oehmcke, S. Remember to Correct the Bias When Using Deep Learning for Regression! *KI - Künstliche Intelligenz* **37**, 33–40 (2023). URL https://doi.org/10.1007/s13218-023-00801-0.

[74] Nord-Larsen, T. *et al.* Forest Plan – pilot project on mapping of forest resources. IGN Report, Department of Geosciences and Natural Resource Management, University of Copenhagen, Frederiksberg, Denmark (2023). URL https://researchprofiles.ku.dk/files/339739375/Forest_plan_mapping_web.pdf.

[75] Nord-Larsen, T., Vesterdal, L., Bentsen, N. S. & Larsen, J. B. Ecosystem carbon stocks and their temporal resilience in a semi-natural beech-dominated forest. *Forest Ecology and Management* **447**, 67–76 (2019). URL https://www.sciencedirect.com/science/article/pii/S0378112719306796.